THE UNIVERSITY OF CALGARY

Region-based Filtering of Multiplicative Noise, Analysis of Edge Sharpness, and Edge Enhancement

by

Arup Das

A THESIS

SUBMITTED TO THE FACULTY OF GRADUATE STUDIES

IN PARTIAL FULFILMENT OF THE REQUIREMENTS FOR THE

DEGREE OF MASTER OF SCIENCE

DEPARTMENT OF ELECTRICAL AND COMPUTER ENGINEERING

CALGARY, ALBERTA

DECEMBER, 1996

ABSTRACT

Image restoration achieved by 3×3 filters may not be effective as they do not take the nonstationary nature of the image into account. We present a new adaptive-neighborhood noise filtering technique for restoring images with multiplicative noise. When evaluated by mean-squared error, the adaptive-neighborhood algorithm produced superior recovery of images degraded by multiplicative noise.

A new method is proposed of computing image edge profile acutance based on the mean-squared gradient along the normals to the boundary of a region of interest (ROI). The acutance algorithm has been tested on different test images, and the resulting values have been found to relate well to the perceived sharpness of the image. Image enhancement techniques are then proposed based on the idea of increasing the acutance of an ROI. The enhancement method has been tested with different blurred test images, and has been found to increase their sharpness as well as the objective measure of acutance.

ACKNOWLEDGEMENTS

I would like to express my sincere appreciation to Dr. Rangaraj M. Rangayyan, my supervisor, for the kind assistance, guidance, and encouragement provided during the entire course of this work, without which the work would have been impossible.

I would also like to acknowledge the support of the Department of Electrical and Computer Engineering and the Natural Sciences and Engineering Research Council (NSERC) of Canada in providing financial assistance for me and for the project.

To my parents, my elder brother Biswarup,

and

to all of my friends.

CONTENTS

LIST OF TABLES

LIST OF FIGURES

LIST OF ABBREVIATIONS

1D - One-Dimensional

2D - Two-Dimensional

AN - Adaptive Neighborhood

ARW - Adaptive Rectangular Window

ATD - Adaptive Two-Dimensional

CMT - Cascaded Modulation Transfer

CMTA - Cascaded Modulation Transfer Acutance

IEP - Image Edge Profile

IEPA - Image Edge Profile Acutance

KESF - Knife Edge Spread Function

LMS - Least Mean Square

LSF - Line Spread Function

MSE - Mean Squared Error

MTF - Modulation Transfer Function

PSD - Power Spectral Density

ROI - Region Of Interest

SAR - Synthetic Aperture Radar

SMT - System Modulation Transfer

SMTA - System Modulation Transfer Acutance

SNR - Signal to Noise Ratio

CHAPTER 1

INTRODUCTION

1.1 Classical Image Processing Techniques

Most images suffer degradation during their formation or recording due to the use of imperfect sensors. Image degradation can be classified in two categories: blur and noise. In general, a degraded image is modeled as the original image convolved with a point spread function plus white noise. Image processing techniques are applied to degraded images to make them more suitable than the original image for a specific application. The established image processing techniques can be broadly classified in the following categories.

1.1.1 Local versus Global Image Processing Techniques

Early attempts to restore noisy images treated the image as a homogeneous random field and used linear global filters for restoration. Global filters can be designed in both the spatial and the frequency domains, and efficiently implemented in a recursive way. However, common global restoration filters essentially operate as global low-pass filters. Therefore, images may be smoothed excessively by these filters, which is especially apparent near edges or at locations of high-frequency information in the image. The human visual system is very sensitive to edges, and hence global methods tend to produce subjectively poor results.

In general, an image is an inhomogeneous random field, and hence it cannot be properly represented by a homogeneous model. Recently, better algorithms for image restoration have been developed by assuming that images are locally stationary. This

means that the local power spectral density (PSD) changes gradually as a small window is moved over the image. A number of experiments by different researchers have shown that the approach based on local stationarity of the image is a significant improvement over the assumption of global stationarity. In most practical image restoration applications, the restoring filter window is relatively small compared to the size of the image. If the image is locally stationary in regions covering at least the spatial extent of the filter window, then the assumption of stationarity is reasonably well justified; consequently, significantly better restored images can be obtained.

1.1.2 Fixed versus Adaptive Image Processing Techniques

Image restoration algorithms can also be classified as fixed and adaptive image restoration techniques. Fixed methods were common in the early periods of image processing, and were designed under the assumption of global stationarity. In fixed methods, the coefficients of the filter as well as the size and shape of the region of support (or application) of the filter remain fixed over the entire image. As the fixed filters do not adapt to changing image characteristics, they tend to smooth the image in order to reduce noise, and thereby blur edges and structured features. To overcome this limitation, a number of adaptive filtering techniques have been proposed. In some adaptive filters, the region of support remains fixed but the filter coefficient values change depending on image characteristics; in some others, the size and shape of the neighborhood over which the filter coefficients are calculated are varied depending on local image characteristics. Adaptive filtering techniques are more complex than fixed techniques and take more computing time to restore images. The finite duration taken by adaptive filters to respond to new image characteristics may affect the filter performance in transition areas of the image. However, adaptive filtering methods take local stationarity of images into account, and the restored images are better as

object edges and other sharp features do not get blurred.

1.2 Scope of the Thesis

This thesis presents various adaptive image restoration and image enhancement techniques where local image characteristics dynamically control the algorithms. In particular, the thesis concentrates on adaptive-neighborhood (AN) image processing techniques which process images using adaptive regions that correspond to areas of the image where relative pixel gray-level differences lie within specified limits of tolerance. The ANs tend to be uniform and tend not to include high-frequency information such as edges. An AN is also called a region.

The main part of the thesis is centered around new AN techniques for image restoration and edge enhancement. In image restoration this thesis deals with only signal-dependent multiplicative noise; however, the concept can be extended to other types of signal-dependent noise such as Poisson noise and film-grain noise. For the edge enhancement part, the thesis presents a method for region-based quantitative measurement of edge sharpness and a new region-based method for improving the edge sharpness of bi-level images. It is shown in the thesis that AN-based image processing techniques work better than those based on fixed-neighborhood techniques.

1.3 Thesis Organization

This thesis is presented in six chapters. Chapter 2 reviews different noise filtering techniques, and gives a detailed review of some of the principal filtering techniques. The general principles of noise filtering are discussed first, both for signal-independent noise and signal-dependent noise. A comparative discussion on local versus global filtering methods, and fixed versus adaptive image restoration methods is presented. Four principal noise restoration filters are discussed in detail, followed by a summary

of the methods.

Chapter 3 presents the proposed AN filter for restoring images with multiplicative noise. The concept of AN processing and the method for finding ANs are described. The structure of the noise filter is presented and discussed. Results of application of the AN multiplicative noise filter are shown, and a comparative analysis (both qualitative and quantitative) with the methods discussed in chapter 2 is provided.

Chapter 4 starts the second part of the thesis which deals with the region-based image enhancement methodology. The chapter starts with reviews on the need for measures of image sharpness and algorithms for computing object edge sharpness. A new method for computing a region-based quantitative measure of object edge sharpness is presented. The method is a modification of an existing algorithm for computing image edge profile acutance. The validity of the algorithm is demonstrated by experimental results.

Chapter 5 presents a new method for enhancing object edge sharpness based on the acutance property of an image. The method is different from the other methods discussed in the thesis that deal with image sharpening in that it does not work on a global basis to enhance the image. Instead, the method sharpens the image by enhancing the edge of each individual object present in the image. The final part of this chapter presents a discussion on experimental results and the comparative merits and demerits of the new technique.

Chapter 6, the final chapter, gives a summarizing discussion on the noise filtering and edge enhancement techniques presented in the thesis and provides suggestions for future work.

CHAPTER 2

NOISE FILTERING

2.1 Principles of Noise Filtering

Noise filtering deals with the problem of recovering an image from its noisy condition. The purpose is to improve the image quality or to obtain some type of information that is not readily available from the original degraded image. Many digital imaging systems introduce noise which cannot be avoided. Film grain, electronic noise, and quantization are some of the major noise sources in digital imaging. Restoration of noisy images has a wide range of applications. In photojournalism and forensic applications, noisy images are very common. In space research, image restoration is becoming an increasingly important aspect because of the inherent noise associated with any optical telescope. In general, the range of image restoration applications is widening with the continuing increase in the use of imaging systems in numerous consumer, commercial, medical, and scientific fields.

The main strategy in noise filtering is to define an estimate of the original image on a quantitative basis and to incorporate a priori information and constraints about the actual image, the blur, and the noise into the estimation process. However, a priori information about the image, the blur, and the noise are often not readily available. Therefore, these quantities need to be modeled and model parameters should be determined properly. The noise process is modeled in two major ways depending on the source and nature of the noise – signal-independent noise and signal-dependent noise.

2.1.1 Signal-independent Noise

In most image restoration algorithms, the observed noise is modeled as additive, white Gaussian noise that is independent of the signal. In this model, the degradation of a digital image is expressed as

$$g(i,j) = h(i,j) * f(i,j) + n(i,j), \tag{2.1}$$

for $i = 0, 1, ..., M-1$, $j = 0, 1, ..., N-1$, the extent of the image formation system. $g(i,j)$ is the observed degraded image, $h(i,j)$ is the image formation system impulse response (or blurring function), $*$ represents two-dimensional (2D) convolution, $f(i,j)$ is the original image, and $n(i,j)$ is a realization of the noise process independent of the signal process represented by $f(i,j)$.

Statistically, noise is considered to be independent of the signal if its statistical characteristics of any order are not a function of the signal or its statistics. Since a Gaussian process is completely characterized by its mean and variance, Gaussian noise is independent of the signal if its first two moments are independent of the signal. Although a non-Gaussian noise process is not completely determined from its first two moments, it may be said to be signal-independent to the second order if its mean and variance are independent of the signal.

The signal-independent noise model has resulted in many successful restoration filters in various areas such as biomedical imaging, television, infrared imaging, space imaging, and industrial radiography. However, it has been well established that a number of image noise sources are signal-dependent (Walkup and Choens [1], Arsenault et al. [2]). Restoration algorithms based on a signal-independent noise model are not expected to be very effective in the signal-dependent noise environment. To restore images from signal-dependent noise, signal-dependent noise models are more appropriate.

2.1.2 Signal-dependent Noise

A number of physical noise processes are inherently signal-dependent. These include photoelectronic shot noise, magnetic tape recording noise, photographic film-grain noise, and speckle noise. Signal-dependent noise sources often have a nonlinear relationship with signal intensity. It has been shown that restoration algorithms which ignore signal dependence of noise pay a penalty in terms of mean squared error (MSE) while trying to restore images from signal-dependent noise [3]. The inclusion of signal dependence in the model, while increasing the complexity of the restoration filters, results in potentially superior performance.

A frequently used model for signal-dependent noise was proposed by Froehlich et al. [3] as

$$g(i,j) = f(i,j) + KF(f(i,j))n(i,j), \tag{2.2}$$

where $g(i,j)$ is the observed degraded image, $f(i,j)$ is the undegraded original image, K is a constant, $F(f(i,j))$ is a function of the undegraded original image $f(i,j)$, and $n(i,j)$ is noise which is independent of the original image $f(i,j)$.

In this thesis, filtering of multiplicative noise will be considered. The degradation by multiplicative noise is modeled as

$$g(i,j) = f(i,j)\, n(i,j), \tag{2.3}$$

where the notations have the same meaning as in equation (2.2). A practical example of multiplicative noise is speckle noise. Coherent illumination results in speckle noise in images acquired by imaging systems with wavelength limitations for detecting very small variations in object roughness. Many coherent imaging systems are widely used, such as ultrasound medical imaging systems, synthetic aperture radar imaging systems for remote sensing, astronomical imaging systems, and laser-illuminated imaging systems. For multiplicative noise, the noisy images have the property that

brighter areas of the image appear to be noisier.

Many filters have been proposed based on signal-independent and signal-dependent noise models for restoring noisy images. They may be classified either as local or global filtering methods, based on whether they take local statistics of the image into account or not. They may also be classified as adaptive or fixed filtering methods, depending on whether or not the algorithms dynamically adapt themselves to the image characteristics.

2.2 Local versus Global Image Filtering Methods

Early image restoration algorithms were designed under the assumption that the image under consideration is a wide-sense 2D stationary random process [4]. The statistical properties of an image, under this assumption, are characterized by its global stationary correlation function, rather than its local statistical properties. Chan and Lim [5] stated that such global algorithms are not successful as most image data that are meaningful to human observers violate the basic assumption of stationarity. Images are typically only quasi-stationary. As global image filtering methods are designed under the assumption of stationarity, they are insensitive to abrupt changes in image intensity, and tend to smooth edges and structured features where the assumption of stationarity is violated [6].

Various algorithms have been proposed to restore images using local statistics. Mean filters [7] restore noisy images, but the edges of the objects are considerably blurred. Median filters [7] can effectively remove discrete impulse noise, but at the cost of greater signal suppression.

Naderi and Sawchuck [8] proposed a nonstationary Wiener filter to remove signal-dependent film-grain noise. Their filter is able to adapt to local signal statistics, given the conditional noise statistics. Lo and Sawchuck [9] derived a nonlinear filter

to restore images affected by Poisson noise. Arsenault and Levesque [10] used the generalized homomorphic transformation to make signal-dependent noise independent of the signal, and combined it with a local-statistics restoration technique to filter images degraded by signal-dependent noise. Lee [11, 12] formulated a local-statistics algorithm using the James-Stein estimator. Jiang and Sawchuck [13] considered the restoration of images degraded by a class of signal-uncorrelated noise, possibly signal-dependent, using the noise-updating repeated Wiener filter; they also investigated other adaptive noise smoothing filters using local image statistics.

2.3 Fixed versus Adaptive Image Filtering Methods

Most of the early image restoration methods were fixed methods, developed using nonrecursive algorithms and implemented in the discrete frequency domain [7]. To deal with images degraded by space-variant blur, methods for 2D extension of the Kalman filtering algorithm [14] and Bayesian estimation were proposed, which led to 2D recursive filtering algorithms.

The constrained least squares filter is an extension of the Kalman filter and was originally proposed by Phillips [15]; refinements and further extensions have been developed by MacAdam [16] and Hunt [17]. Another approach to image restoration is homomorphic filtering, which was introduced in one-dimensional (1D) signal-processing by Oppenheim et al. [18].

Fixed filtering methods often tend to smooth out edges because of the inherent assumption of a stationary image model. Many adaptive restoration systems have been proposed to rectify this problem. Ingle et al. [19] allowed the parameters describing the image model to change within the image, and derived an identification-estimation algorithm. Ingle and Woods [20] considered the case of five models (describing edges of different orientations), and developed a multiple-channel estimation algorithm. Us-

ing a totally different approach, Peyrovian and Sawchuck [21] derived nonstationary, nonrecursive filters that provide a compromise between loss of resolution around edges and the effect of noise in smooth regions. Rajala and Figueiredo [22] proposed a 2D recursive filter assuming a piecewise-stationary model for the image. The image was first segmented into disjoint regions based on local spatial activity and a different Kalman filter was used for nonstationary restoration of each region. Their method emphasized nonstationarity within regions.

Lev et al. [23] suggested a 3×3 kernel that is contextually set depending on local image characteristics. Prager [24] used a simplified form of this technique for noise suppression and called it conditional smoothing. Nagao and Matsuyama [25] proposed an algorithm which selects the most homogeneous neighborhood and replaces each pixel by its neighborhood average. Such adaptive algorithms are most suitable for smoothing noise in images with strong edges as a preprocessing step for future segmentation. However, subtle details, such as thin lines and small but distinguishable objects, are suppressed by these methods.

In the following chapters we will discuss a few adaptive restoration algorithms in more detail. Subsequently (in chapter 3), we will compare the results obtained by these methods with the results obtained by our proposed method, when applied on the same test images.

2.4 The Adaptive Two-dimensional LMS Algorithm

Hadhoud and Thomas [26] and Mikhael and Ghosh [27] proposed an efficient algorithm they called the adaptive two-dimensional least-mean-squares (ATD LMS) method. The method uses a causal finite impulse response (FIR) filter $W_p(i,j)$ whose region of support is $M \times M$ (M is typically 3) such that

$$\hat{f}(i,j) = \sum_{k=0}^{M-1} \sum_{l=0}^{M-1} W_p(k,l) g(i-k, j-l), \tag{2.4}$$

where $\hat{f}(i,j)$ is the restored value of the pixel (i,j), $g(i,j)$ is the noise-corrupted input image, and p marks the current position of the restoration filter in the input image computed as

$$p = iN + j, \tag{2.5}$$

for the pixel position (i,j) in an $N \times N$ image, and takes values from 0 to $N^2 - 1$. The filter coefficients $W_{p+1}(i,j)$ at the next pixel position $(p+1)$ are determined by minimizing the MSE at the pixel location p, using the steepest descent algorithm, and are computed as

$$W_{p+1}(i,j) = W_p(i,j) - \mu \Delta_p(e_p^2), \tag{2.6}$$

where μ is the convergence and filter stability factor, e_p is the difference between the desired signal and the estimated signal, and Δ_p is a gradient operator applied to e_p^2 at the pixel location p.

The error signal e_p is given by

$$e_p = f(i,j) - \hat{f}(i,j). \tag{2.7}$$

Since the original image is unknown, the error signal e_p is typically obtained by applying a 2D delay operator of $(1,1)$ samples to the degraded image in order to approximate the original image $f(i,j)$.

Combining equations (2.4), (2.6), and (2.7), we get

$$W_{p+1}(i,j) = W_p(i,j) + 2\mu e_p \Delta_p g(i-k, j-l). \tag{2.8}$$

The convergence factor μ is determined by trial and error. The ATD LMS algorithm implemented by Rabie [28] is used in this thesis for comparative analysis. The ATD LMS algorithm tends to reduce the noise uniformly across the entire image, which

leads to smoothing of edges. Decreased sharpness of edges normally makes images less pleasing to the viewer.

2.5 The Adaptive Rectangular Window LMS Algorithm

Song and Pearlman [29, 30] proposed a method of adaptive estimation in which the size of the neighborhood over which filter coefficients are calculated is varied. The method was refined later by Mahesh et al. [6]. In their method, the same noisy image model as in equation (2.1) is used, with the additional assumption of no blurring, that is $h(i,j) = 1$. The noise $n(i,j)$ is assumed to be of zero mean and variance σ_n^2 and uncorrelated to the original signal $f(i,j)$, which is assumed to have mean m_f and variance σ_f^2. The estimate of the original signal is given by

$$\hat{f}(i,j) = \alpha\, g(i,j), \tag{2.9}$$

and the factor α at each pixel location is found by using the minimum MSE criterion of the standard Wiener filter. The error is given by

$$e(i,j) = f(i,j) - \hat{f}(i,j) = f(i,j) - \alpha\, g(i,j). \tag{2.10}$$

A necessary and sufficient condition for the minimization of the MSE is that the error signal $e(i,j)$ should be orthogonal to the original signal $g(i,j)$, that is,

$$E\{[f(i,j) - \alpha\, g(i,j)]g(i,j)\} = 0, \tag{2.11}$$

where $E\{.\}$ is the expectation operator. The solution of equation (2.11) gives the value of α as

$$\alpha = \frac{\sigma_f^2}{\sigma_f^2 + \sigma_n^2}, \tag{2.12}$$

which is a first-order LMS estimator at each point in the image. If the original image has a non-zero mean, then the estimator is found by first subtracting the mean from both of the images $f(i,j)$ and $g(i,j)$. Since the mean of the noise is zero, the a

posteriori mean m_g of the image $g(i,j)$ at pixel position (i,j) is equal to the a priori mean m_f of the original image $f(i,j)$. Then, the first-order LMS estimate is given as

$$\hat{f}(i,j) = m_g + \frac{\sigma_f^2}{\sigma_f^2 + \sigma_n^2}[g(i,j) - m_g]. \tag{2.13}$$

The ARW algorithm starts with the window size of 1×1 for the pixel (1,1). Then, two thresholds T_i and T_j are defined as

$$T_i = \frac{7\sigma_n^2}{n_i}, \qquad T_j = \frac{7\sigma_n^2}{n_j}, \tag{2.14}$$

where n_i and n_j are the lengths of the ARW in the i and j directions, respectively. The variances of the signal in the current row (σ_r^2) and the current column (σ_c^2) are then computed as

$$\sigma_r^2 = \sigma_i^2 - \sigma_n^2, \qquad \sigma_c^2 = \sigma_j^2 - \sigma_n^2, \tag{2.15}$$

where σ_i^2 and σ_j^2 are the values of the variance in the input image calculated over n_i and n_j pixels in the i and j directions, respectively. These variances are then compared with the arbitrarily-defined thresholds given by equation (2.14). If the variance in the i (or j) direction is greater than the corresponding threshold, then the ARW size is progressively increased in that direction; otherwise, it is decreased. The ARW is restricted to a maximum of 11×11 pixels to ensure that each ARW corresponds to a relatively homogeneous region in the image.

The implementation of the ARW algorithm by Rabie [28] is used in this thesis for comparative analysis. The ARW LMS method typically smooths uniform regions of the image with a large window, but leaves the image almost unchanged in regions containing edges or high spatial variance. The resulting image generally has more noise at edges than in uniform regions. However, since human observers are typically able to tolerate more noise at edges than in smooth areas, the resultant image could be more pleasing than the noisy image [6].

2.6 The Adaptive-neighborhood Noise Subtraction Algorithm

The adaptive-neighborhood noise subtraction (ANNS) algorithm was proposed by Paranjape et al. [31]. The method operates on the same general principle as the ARW LMS algorithm; however, the window size is not necessarily a rectangular one as in the ARW LMS algorithm. In the ANNS method, the estimate of the additive noise is computed on the basis of a variable-size, variable-shape AN for each pixel in the input image.

In the ANNS algorithm, the degraded image is represented by a zero-mean random variable $f(i,j)$ of variance σ_f^2 with no blurring. The degraded image is represented as (from equation (2.1))

$$g(i,j) = f(i,j) + n(i,j), \tag{2.16}$$

where the noise $n(i,j)$ is of zero mean, of variance σ_n^2, and is uncorrelated to $f(i,j)$. An estimate of the additive noise, $\hat{n}(i,j)$ is then computed using the pixels in an AN as

$$\hat{n}(i,j) = \beta[g(i,j) - m_\alpha], \tag{2.17}$$

where m_α is the mean value computed over the AN and β is a scale factor computed in the following way.

Using the estimate of the noise in equation (2.17), an estimate of $f(i,j)$ is computed as

$$\hat{f}(i,j) = m_\alpha + (1-\beta)[g(i,j) - m_\alpha]. \tag{2.18}$$

From equation (2.17), σ_n^2 is expressed as

$$\sigma_n^2 = \beta^2 \sigma_g^2. \tag{2.19}$$

From equation (2.16), it can be shown that

$$\sigma_g^2 = \sigma_f^2 + \sigma_n^2. \tag{2.20}$$

Combining equations (2.19) and (2.20), we get

$$\sigma_n^2 = \beta^2(\sigma_f^2 + \sigma_n^2), \tag{2.21}$$

where σ_f^2 is the estimated signal variance given by

$$\sigma_f^2 = \sigma_{AN}^2 - \sigma_n^2, \tag{2.22}$$

where σ_{AN}^2 in turn is the variance of the AN. Then, β is given by

$$\beta = \left(\frac{\sigma_n^2}{\sigma_f^2 + \sigma_n^2}\right)^{1/2}. \tag{2.23}$$

From equation (2.18), the final estimate for the original image is obtained as

$$\hat{f}(i,j) = m_\alpha + \left[1 - \left(\frac{\sigma_n^2}{\sigma_f^2 + \sigma_n^2}\right)^{1/2}\right][g(i,j) - m_\alpha]. \tag{2.24}$$

The AN is formed for each pixel of the image in such a way that it defines a relatively uniform region in the image. Identification of the AN will be discussed in more detail later in this thesis. An implementation of the ANNS by Paranjape et al. [31] is used in this thesis for comparative analysis.

2.7 The Fixed-neighborhood Multiplicative Noise Filter

A fixed-neighborhood filter for multiplicative noise was proposed by Kuan et al. [32]. The filter algorithm starts with the additive noise model given by equation (2.1). If the conditional mean of the noise given the signal is zero, that is

$$E\{\mathbf{n}|\mathbf{f}\} = \mathbf{0}, \tag{2.25}$$

where $\mathbf{n}$ and $\mathbf{f}$ represent the noise and signal processes, respectively, the adaptive linear minimum mean squared error estimate of the signal is given by [32]

$$\hat{f}(i,j) = E\{f(i,j)\} + \frac{v_f(i,j)}{v_f(i,j) + \sigma_n^2(i,j)}[g(i,j) - E\{g(i,j)\}], \tag{2.26}$$

where $\sigma_n^2(i,j)$ is the nonstationary noise ensemble variance at the pixel location (i,j); $E\{f(i,j)\}$ and $E\{g(i,j)\}$ are the ensemble means of $f(i,j)$ and $g(i,j)$, respectively; and $v_f(i,j)$ is the local spatial variance of $f(i,j)$.

For multiplicative noise, the same filter in equation (2.26) can be used. However, the multiplicative noise variance cannot be used directly, as the noise is not additive; instead, $\sigma_n^2(i,j)$ is computed in the following way. The degradation model for the multiplicative noise model can be written as (using a different notation than that used in equation (2.3)) [32]

$$g'(i,j) = f(i,j)\,u(i,j), \tag{2.27}$$

where $u(i,j)$, the multiplicative noise, is independent of $f(i,j)$. The observation is normalized by the known noise mean as

$$g(i,j) = g'(i,j)/E\{\mathbf{u}\}, \tag{2.28}$$

where $\mathbf{u}$ is the noise process, and $E\{\mathbf{u}\}$ is the noise mean. Expressing equation (2.28) in terms of signal plus signal-dependent additive noise, the additive noise is found as [32]

$$n(i,j) = \left[\frac{u(i,j)}{E\{\mathbf{u}\}} - 1\right] f(i,j). \tag{2.29}$$

The additive noise variance is

$$\sigma_n^2(i,j) = \frac{\sigma_u^2\left[[E\{f(i,j)\}]^2 + \sigma_f^2(i,j)\right]}{[E\{\mathbf{u}\}]^2}, \tag{2.30}$$

where σ_u^2 is the noise variance, and $\sigma_f^2(i,j)$ is the ensemble signal variance. It can be verified that the noise $n(i,j)$ in equation (2.29) satisfies the condition in equation (2.25). Replacing ensemble statistics in equations (2.30) and (2.26) by local spatial statistics and using the value of $\sigma_n^2(i,j)$ from equation (2.30) in equation (2.26), Kuan et al. [32] proposed the following adaptive noise smoothing filter for the multiplicative

noise model:

$$\hat{f}(i,j) = \bar{f}(i,j) + \frac{v_f(i,j)[g(i,j) - \bar{f}(i,j)]}{v_f(i,j) + \sigma_u^2[(\bar{f}(i,j))^2 + v_f(i,j)]/[E\{u\}]^2}, \tag{2.31}$$

where $\hat{f}(i,j)$ is the filter output for the pixel location (i,j), $g(i,j)$ is the normalized observation, $\bar{f}(i,j)$ is the local 3×3 mean, and $v_f(i,j)$ is the local 3×3 variance.

From equation (2.31), it is seen that the filter adapts itself to local variations in image statistics. The implementation of the filter shows that the filter is noise smoothing; however, the filter blurs object edges to some extent as it operates on 3×3 neighborhoods. The filter works better than the ATD LMS, the ARW LMS and the ANNS algorithms in restoring images with multiplicative noise.

2.8 Summary

In this chapter, the principles of noise filtering and some of the existing restoration filters were discussed. In particular, mean and median filters, the ARW LMS algorithm, the ATD LMS algorithm, the ANNS algorithm, and the 3×3 multiplicative noise filter of Kuan et al. were discussed in detail, as we will compare their performance with that of our proposed method later in this thesis. It should be noted that the ARW LMS, the ATD LMS, and the ANNS algorithms are not expected to work well in the presence of multiplicative noise as they were designed for restoring images with additive noise. The algorithms were chosen for comparative analysis as they represent powerful adaptive methods. The 3×3 multiplicative filter, on the other hand, was designed to restore images with multiplicative noise; however, the filter suffers from the same limitations as any 3×3 image processing technique. The next chapter shows that the multiplicative noise filter can be improved if it is applied on the basis of ANs instead of 3×3 neighborhoods. It is also shown that the restoration method works better as the computer-generated variable-size, variable-shape regions match more closely with visually identifiable regions in the image.

CHAPTER 3

ADAPTIVE-NEIGHBORHOOD FILTERING OF MULTIPLICATIVE NOISE

In this chapter a new adaptive-neighborhood restoration filter to restore images degraded by multiplicative noise is proposed. The filter uses statistics computed over adaptive-neighborhoods which are grown to include statistically stationary regions with similar gray levels. The method is a new algorithm for restoring images degraded by multiplicative noise using the adaptive-neighborhood image processing paradigm which was first proposed by Gordon and Rangayyan in 1984 [33].

3.1 Adaptive-neighborhood (AN) Image Processing

In AN image processing, an AN is defined about *each* pixel in the image, the extent of which is dependent on the characteristics of the image feature in which the given pixel is situated. Such a neighborhood of similar pixels is called a region. In image segmentation, groups of pixels are found that have some property in common (such as similar gray level) and are used to define disjoint image regions. AN processing may be performed by initially segmenting the given image and then processing each segment in turn. Alternatively, AN processing may define possibly overlapping regions for each pixel and process each of these regions independently. Then, features in the image are processed as units, rather than pixels being processed using arbitrary groups of neighboring pixels (for example 3×3 masks). Image processing procedures can then be applied on an image feature basis, rather than on a pixel-by-pixel basis.

3.1.1 Region Growing

The fundamental step in AN image processing is defining the extent of regions in the image. Of the two classes of regions, namely non-overlapping regions obtained using image segmentation techniques, and overlapping regions obtained from region growing techniques, overlapping regions are used in the proposed method, as processing disjoint segments of an image may result in noticeable edge artifacts and an inferior restored image.

The region growing method used in the proposed filter is based on a simple graphical seed-fill algorithm, known as pixel aggregation [34]. Details of implementation of the method may be found in the paper by Morrow et al. [35]. In this method, regions consist of connected pixels that fall within a specified gray-level deviation from the starting or seed pixel. Either 8-connectivity or 4-connectivity may be used. 8-connectivity has been used here, as it has been found to result in more accurate matches between the regions grown and visually identifiable objects.

The AN is defined using 8-connected region growing and a pre-specified tolerance about the seed pixel's gray level. The tolerance is defined as

$$\frac{|p(k,l) - p(i,j)|}{p(i,j)} \leq t, \tag{3.1}$$

where $p(i,j)$ is the gray level of the seed pixel (i,j) and $p(k,l)$ is the gray level at the connected pixel (k,l). The tolerance t is given as a fraction of the seed pixel's gray level, and determines the maximum gray-level deviation allowed within the region.

For each seed pixel, the tolerance t is initially set to 0.01 (allowing 1 percent

deviation about the seed pixel's value). If the number of pixels in the region grown is less than four, then the tolerance is increased by 0.01. The process is continued until a region is grown with four or more pixels, or the tolerance reaches a maximum value of 0.4. Any deviation less than the tolerance level is considered to be an intrinsic property of the region, or to be noise.

An AN typically groups pixels that are similar to the seed pixel in terms of both gray level and proximity (connectivity). These pixels are usually contextually related and are likely to belong to the same object or region. Figure 3.1(a) shows an actual AN region grown from the seed pixel at location (76, 83) in a synthesized test image (the characteristics of the synthesized test image will be described later in subsection 3.3.1). The AN exactly matches the part of a circular object of the image (not overlapped by neighboring objects) which contains the seed pixel. Figure 3.1(b) shows an AN region grown from the seed pixel at location (58, 73) in the hat region of the Lenna image. The region grown includes a uniform region surrounding the seed pixel. Figure 3.1(c) shows the region grown from the seed pixel at the location (165, 43). The seed pixel lies in the mane region of the Lenna image and the region contains texture. The AN grown is very small. Any textured region contains many different adjacent high-frequency pixel ensembles. As the AN grown tries to identify a *uniform* region and tends to avoid edges and other nonstationary areas present in a textured region, the size of the AN grown is likely to be small in textured areas.

As mentioned at the beginning of this subsection, the ANs can be overlapping. Figure 3.2 shows an example of two overlapped regions in a noisy version of the

Lenna image. The first AN was grown from the seed pixel at the location (153, 135) and the boundary of the AN is marked white. The second AN was grown from the seed pixel at the location (165, 134) and the boundary of the AN is marked black. The two ANs encompass two different uniform regions with significant overlap.

The basic idea in an AN filter is to apply filtering methods based on the statistics of adaptive regions whose size and shape are based on the structural information content of the image, rather than of arbitrarily formed rectangular regions. It should be noted that *each* pixel in the given image is treated as a seed pixel for region growing and filtering.

3.2 Local Statistics-based Filter for Multiplicative Noise

In the proposed AN method, the same filter structure as in equation (2.31) is used. However, the statistics used in the filter are not computed over a 3×3 neighborhood; instead they are computed over the AN for each pixel for the reason described below.

Any restoration filter filters noise by replacing the pixel value by a certain average computed over a predefined neighborhood. Mathematically, ensemble statistics are used as the parameters of the filters. However, in practice, the ensemble statistics are not available. Often, the ensemble statistics are approximated by local statistics under the assumption that the pixels within the averaging neighborhood are from the same ensemble. However, if there is a high-frequency component in the averaging window, the sample variance tends to overestimate the ensemble variance, because samples in two entirely different ensembles are used to calculate the sample variance.

The sample variance is much higher than the ensemble variance in a high-frequency region of the image. The sample mean is also inaccurate.

The effects of inaccurate estimates of signal mean and signal variance can be explained from the structure of an image. Many researchers have proven that images cannot be modeled as wide-sense stationary process and that the statistical properties of an image cannot be characterized by its global stationary statistics. A more accurate model was given by Kuan et al. [32], where the image is described by a nonstationary mean, nonstationary variance process. The nonstationary mean accounts for the general structure of the image, whereas the nonstationary variance characterizes the high-frequency components of the image, e.g., edges and textures. It may now be seen that an inaccurate signal variance has a severe effect on the restored image as it tends to obscure the high-frequency information in the image and the edges get blurred. If an inaccurate mean is used to describe the gross structure of the image, the effect of the nonstationary mean is not prominent in the restored image, as it may only affect the relative brightness or intensities of objects.

To avoid this problem, the ANs (discussed in section 3.1) are grown in such a way that they include uniform areas only and do not include edges. For a uniform region, the regions grown include the pixels which tend to belong to the same object or ensemble only (figure 3.1(b)). For a textured region where there are many high-frequency components, the size of a typical AN is usually very small in order to avoid including two different pixel ensembles or components of the texture in the same AN or averaging neighborhood. Therefore, it can be expected that AN mean and

AN variance provide better estimates of the ensemble mean and ensemble variance, respectively.

In the proposed filter for multiplicative noise, the ensemble signal mean $E\{f(i,j)\}$, and the ensemble signal variance $\sigma_f^2(i,j)$ are approximated by the AN mean $m_{AN}(i,j)$, and the AN variance $\sigma_{AN}^2(i,j)$, respectively. The filter is then given by

$$\hat{f}(i,j) = m_{AN}(i,j) + \frac{\sigma_{AN}^2(i,j)[g(i,j) - m_{AN}(i,j)]}{\sigma_{AN}^2(i,j) + \sigma_u^2[(m_{AN}(i,j))^2 + \sigma_{AN}^2(i,j)]/[E\{\mathbf{u}\}]^2}, \tag{3.2}$$

where $\hat{f}(i,j)$ is the filter output for the pixel location (i,j) and $g(i,j)$ is the normalized observation. The factor $[(m_{AN}(i,j))^2 + \sigma_{AN}^2(i,j)]$ is an index of the signal-dependent properties of the multiplicative noise, and the presence of this factor shows how the filter adapts itself to smooth the signal-dependent noise. The factor $\sigma_u^2/[E\{\mathbf{u}\}]^2$ denotes the multiplicative noise level.

To understand the behavior of the filter, a filter control factor can be defined as

$$C = \frac{\sigma_{AN}^2(i,j)}{\sigma_{AN}^2(i,j) + \sigma_u^2[(m_{AN}(i,j))^2 + \sigma_{AN}^2(i,j)]/[E\{\mathbf{u}\}]^2}, \tag{3.3}$$

so that the filter in equation (3.2) can be rewritten as

$$\hat{f}(i,j) = m_{AN}(i,j) + C * [g(i,j) - m_{AN}(i,j)]. \tag{3.4}$$

If the noise is high, then σ_u^2 is comparable to $[E\{\mathbf{u}\}]^2$ and C is low (from equation (3.3)). Then, the filter in equation (3.4) puts more weight on the a posteriori mean $m_{AN}(i,j)$. In this situation, the observation is very noisy, and the a posteriori averages are used to smooth the noise. In the case of low noise, σ_u^2 is very small compared to $[E\{\mathbf{u}\}]^2$. Then, from equations (3.3) and (3.4), we can see that the filter puts more

weight on the noisy observation $g(i,j)$ and edges are preserved better as a result of less averaging.

3.3 Results

In order to test the proposed method, 3×3 mean and median filters [7], the ATD LMS algorithm [26], the ARW LMS algorithm [29, 30], the ANNS algorithm [31], the 3×3-neighborhood multiplicative noise filter of Kuan et al. [32], and the proposed AN multiplicative noise filter were applied to two synthesized test images and two natural images after they had been contaminated with multiplicative, white Gaussian noise. The resultant images were analyzed by visual examination and by calculation of the MSE between the original and the restored images. The visual quality of each filtered image was judged by the author by observing the extent of noise reduction in smooth regions, and by observing the retention of sharp edges as well as textual details in the image.

3.3.1 Generation of Synthesized Test Images

Two synthesized test images were generated in order to test the AN algorithm. The first synthesized test image (figure 3.3(a)) is a 128×128 image containing many objects in the form of rectangles, circles, and triangles of various gray levels and size. The objects are placed at randomly-selected positions. The gray level values of the objects vary from 0 to 255, with the background being a constant of 60. Figure 3.3(b) shows the degraded image with signal-dependent multiplicative white noise of mean

0.5 and variance 0.007. Since the noise is multiplicative, the noisy image has reduced intensity, by an average factor of 2 (reciprocal of the noise mean). The noisy image may be normalized by dividing each pixel of the image by the known noise mean. The MSE between the normalized noisy image and the original image is 382.5. The test image has a number of almost-ideal edges, which are useful for observing the edge-degrading characteristics of the different algorithms.

The second synthesized test image was prepared in a manner similar to the first synthesized image. However, the uniform background of the image has a gray level value of 65. The image was corrupted by signal-dependent multiplicative Gaussian noise of mean 1 and variance 0.05. Figures 3.4(a) and 3.4(b) show the original and noisy versions of the second synthesized test image. Since the noise mean is 1 here, the noisy image need not be normalized for MSE calculation. The MSE between the original and noisy versions of the second synthesized image is 100.2.

3.3.2 Restoration of Synthesized Images

Figures 3.3(c) to 3.3(f) show the different restored images for the first synthesized image. Images restored by the 3×3 mean filter, the ARW LMS filter, the 3×3 filter of Kuan et al., and the AN method are displayed for comparison. The mean filter results in a considerably blurred image, as shown in figure 3.3(c). The image produced by the 3×3 median filter (not shown) was better than the image restored by the 3×3 mean filter both in terms of edge sharpness and noise retained in the images. However, both the images show that simple, conventional 3×3 techniques fail to restore images

affected by signal-dependent multiplicative noise without blurring.

The ATD LMS method (result not shown) performed almost as poorly as the 3×3 mean and median filters. The convergence factor used in the ATD LMS algorithm was 40×10^{-9}; the value was selected after many trials. The output image was significantly blurred with most of the noise largely intact. The ARW LMS-restored image is presented in figure 3.3(d). The ARW size was restricted to be a minimum of 1×1 and a maximum of 5×5. The image appears to be noisier than the other restored images. Both the ATD LMS and the ARW LMS methods are designed for restoring images with additive noise, and failed to restore images contaminated with multiplicative noise.

The ANNS method restores the image on the basis of ANs, instead of rectangular neighborhoods. The filter used in the ANNS method was specifically designed for signal-independent additive Gaussian noise. The ANNS method also failed to restore the image affected by signal-dependent multiplicative noise (result not shown).

The output of the 3×3 multiplicative noise filter of Kuan et al. [32] is shown in figure 3.3(e). The image appears to be better than the other restored images discussed so far. However, considerable noise is still present in the restored image. The noise is prominent both in the uniform background and within the objects.

Figure 3.3(f) shows the image restored by the AN method. The image was obtained after four iterations of the AN method (iterating the AN method is discussed in subsection 3.3.3). The uniform regions in the image contain much less noise in the restored image than in the input image or any of the other filtered images. The noise

is more prominent in some of the brighter objects of the image. On the other hand, in the case of very-low-contrast regions, the regions may not be visible after filtering. In spite of these limitations, the image restored by the AN method is clearly the best restored image based on direct visual examination of the filtered images in figure 3.3.

The MSE values between the original and the restored images are listed in table 3.1. The 3×3 filter of Kuan et al. and the AN method perform normalization of the restored image as part of the algorithm. For the other restored images, the results were normalized by the known noise mean before computing the MSE (the MSE values would be much larger without the normalization step). From the table, it is seen that the image restored by the AN method has the lowest MSE in the series of images and methods considered. Thus, the AN method appears to be the best of all the methods studied, both qualitatively and quantitatively for images degraded by multiplicative white Gaussian noise.

A similar set of tests was performed on the second synthesized test image, and figure 3.4 presents some of the results obtained. Only the original and noisy images, and the results of the 3×3 filter of Kuan et al. and the AN method are shown. The MSE values for the second synthesized image are also listed in table 3.1. Visual inspection of the images in figure 3.4 and their MSE values indicate that the AN method consistently produces better restored images than those generated by the other algorithms for the synthesized test images.

3.3.3 Repeated Application of the AN Algorithm

Repeated application is a powerful and useful attribute of the AN image filtering methods, which was first proposed by Paranjape et al. [36] and used in their ANNS algorithm [31] and the AN mean and median filters [37]. For iterative application of the filters, knowledge of noise variance is required at each pass through the filter. In the present study, it was found that the original noise variance works well for successive iterations as well. Thus, no additional information is used in the successive iterations.

Figure 3.5 displays the results of repeated application of the AN method for the first synthesized image. The MSE values of the restored images after successive iterations are listed in table 3.2. From the table it is seen that the MSE value continues to decrease until the fourth iteration, after which it starts to increase. Thus, the AN method may be iterated and the MSE observed after each iteration. When the MSE starts to increase, processing may be stopped, and the restored image obtained from the previous iteration taken as the final restored image. For the first synthesized image, the restored image obtained after the fourth iteration of the AN method was taken as the final restored image. The final restored image (figure 3.5(f)) is seen to be almost free of noise. The successive iterations restore the images without any blurring of the edges of the objects in the image.

Figure 3.6 shows regions grown for the same seed pixel (with co-ordinates (52, 94)) for the original, noisy, and the restored images obtained after the first few iterations of the AN algorithm. The same region growing criterion as given in equation (3.1)

was used for all the images. The images show that the region grown for the original image (figure 3.6(a)) includes exactly the object containing the seed pixel. For the noisy image, the region grown (see figure 3.6(b)) is small, and does not cover much of the object containing the pixel. After the first iteration, the region grown for the same seed pixel (see figure 3.6(c)) includes three different objects (two other objects besides the object containing the seed pixel). The region grown for the restored image obtained after the second iteration (not shown) is almost the same as that after the first iteration. After the third iteration, however, the region grown (see figure 3.6(d)) includes only two objects (one other object besides the object which contains the seed pixel). The region grown for the restored image obtained after the fourth iteration (figure 3.6(e)) includes only the object in which the seed pixel is located. After the fifth iteration, the region grown (figure 3.6(f)) again includes another object in addition to the object containing the seed pixel. The images in figure 3.6 and the MSE values listed in table 3.2 suggest that as regions are identified better (i.e. as the regions grown are more properly matched with the objects in the image), the AN method works better in noise removal. It should be noted that the regions grown for the original image and for the image obtained after the fourth iteration (the regions illustrated in figures 3.6(a) and 3.6(e)) are almost identical for the same seed pixel under consideration.

For the second synthesized image, the MSE started to increase after the second iteration of the AN method. The MSE after the first pass of the AN method is the lowest of all the restored images obtained in this study (see table 3.1), and the best

restored image is obtained after the very first pass of the AN method.

3.3.4 Restoration of Natural Images

Figure 3.7 presents results obtained with the commonly-used Lenna image. The original image is a 256×256 image with gray levels ranging from 0 to 255, and is shown in figure 3.7(a). The Lenna image was corrupted with multiplicative noise of mean 1 and variance 0.05; the corrupted image is shown in figure 3.7(b), which has an MSE of 882.8. The results of the 3×3 median, ATD LMS, 3×3 multiplicative noise filter of Kuan et al., and the AN filters are presented in figures 3.7(c) - 3.7(f). The convergence factor used for the ATD LMS algorithm was 40×10^{-9}. The AN method was iterated until the MSE started to increase; for the Lenna image, the minimum MSE was achieved after 3 iterations. Again, the final restored image produced by the AN method is clearly the best output image based on direct visual examination of the different restored images.

The MSE values between the original and the restored versions of the Lenna image are shown in table 3.3. The ATD LMS method suppressed the noise to some extent without blurring the image. The restored images produced by the 3×3 median filter and the filter of Kuan et al. also have low MSE values compared to that of the noisy image. The median filter-restored image is, however, badly blurred. The AN method has produced the restored image with the least MSE value and the best visual quality.

Figure 3.8 shows the regions grown for the Lenna image for a particular seed pixel (co-ordinates (153, 135)) for the original, noisy, and the restored images obtained

after each of the first three iterations of the AN method. It is seen that the region grown in the noisy image is very small, and that after each iteration of the AN filter, the region grows bigger. The region grown for the restored image obtained after the second iteration matches most closely with the region grown for the original image for the same seed pixel. The MSE attains its lowest value after the third iteration of the filter (note that the third iteration of the filter is applied on the basis of regions grown on the restored image obtained after the second iteration).

After the third iteration, the region grows much larger, and includes other visually different regions in the image; the MSE starts to increase at the same time. These results suggest that optimal restoration of the noisy image is achieved when the regions identified by the AN method match closely with actual regions in the original image.

All of the restoration methods under consideration were applied to another natural image (Sarah), which is of a girl sitting on a beach. The size of the image is 128×128 and the gray level values range from 0 to 255. The image was corrupted by multiplicative noise of mean 1 and variance 0.01. Figure 3.9(a) and 3.9(b) show the original and noisy images, respectively. The image contains some very bright areas where the multiplicative noise looks very prominent, in the form of black dots. The MSE of the noisy image is 679.2.

Figures 3.9(c) and 3.9(d) show the restored images given by the 3×3 filter of Kuan et al. and by the AN method, respectively. The minimum MSE was achieved after two iterations of the AN method. From visual inspection (by the author only) of the

restored images, it is seen that the AN method does not work well in removing the black spots from the bright regions of the noisy image (e.g. the hat and the upper arm); however, the method still gives the best restored image in the present study. The MSE values of the different restored images for the Sarah image are listed in table 3.3. Again, the restored image obtained by the AN method has the least MSE value.

It should be mentioned here that the AN filter did not work consistently as well in textured regions as in uniform regions of the test images. For example, the MSE value computed over a 24×12 area in the mane region (figure 3.10(a)) of the restored Lenna image obtained by the AN method is 480.1, whereas the MSE value for the same area in the noisy Lenna image is 571.0. The MSE value computed over the same area of the restored Lenna image obtained by the 3×3 filter of Kuan et al. is 339.2. The MSE value computed over a 28×9 area in the sand region (figure 3.10(b)) of the restored Sarah image obtained by the AN method is 112.5; the MSE values computed over the same area for the noisy and the restored image obtained by 3×3 filter of Kuan et al. are 415.8 and 217.2, respectively.

On the other hand, the MSE value computed over a 19×14 area which contains two uniform regions with a distinct edge between the regions (figure 3.10(c)) of the restored Lenna image obtained by the AN method is 154.4. The MSE value for the same area in the noisy Lenna image is 921.5, and that of the restored Lenna image obtained by the 3×3 filter of Kuan et al. is 380.7. The same trend was observed in a few regions containing edges for the Sarah image also.

Finally, the MSE value computed over a 16×11 area containing a uniform region with no edges (figure 3.10(d)) of the restored Lenna image obtained by the AN method is 48.6. The MSE values computed over the same area for the noisy Lenna image and the restored image obtained by 3×3 filter of Kuan et al. are 1005.1 and 276.9, respectively. For the Sarah image also, the MSE values computed over rectangular areas containing uniform regions (with no edges and textures) for the restored image obtained by the AN method were found to be consistently much lower than the corresponding MSE values for the restored image obtained by the 3×3 filter by Kuan et al.

From the above discussion it may be concluded that the AN method works better than the 3×3 multiplicative filter of Kuan et al. in uniform regions and regions containing edges, both qualitatively and quantitatively. However, the method may not always work better than the 3×3 filter of Kuan et al. in textured areas. A more sophisticated region growing criterion tailored for textured regions may further improve the performance of the AN filter. Regardless, the MSE computed over the entire image was consistently the lowest for the AN-restored image in all experiments conducted in this study.

3.4 Summary

We have proposed a new method for restoring images corrupted by signal-dependent multiplicative noise. The method is based on applying an adaptive local-statistics-based filter over adaptive-neighborhoods. The filter has a very simple structure and

does not require any a priori information about the original image. The noise mean and variance required may be easily obtained from other data or by other methods. The method consistently produces better restored images than the 3×3 mean, 3×3 median, ATD LMS, ARW LMS, and ANNS filters, as well the 3×3 multiplicative noise filter of Kuan et al., in terms of both visual quality and MSE. The AN method was further applied in a multi-pass procedure, and was observed to provide superior performance with the least MSE for two synthesized test images and two natural images. The AN method restores images without blurring edges. The method also works well for removing noise around edges and other sharp features in the image. The AN method takes into account the nonstationarities of the given image, and the success of the method relies on identifying actual regions and objects present in the image. The method is most suitable for restoring images which are originally piece-wise stationary.

The AN approach can be successfully applied to obtain a quantitative measurement of object edge-sharpness and for image enhancement as well, by sharpening the edges of the objects present in the image. This will be discussed in the following chapters.

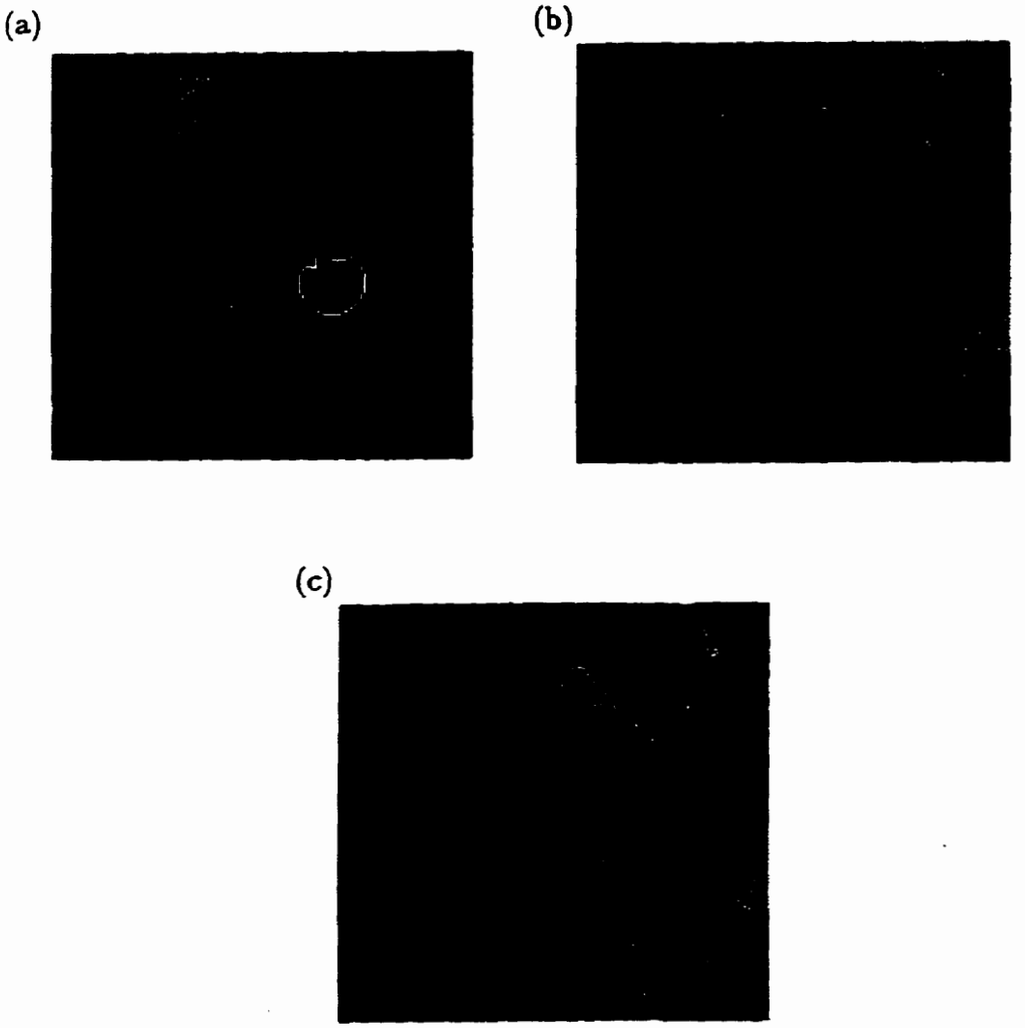

Figure 3.1. ANs grown in two test images (outlined in white):
(a) With seed pixel (76, 83) for a synthesized test image of size 128×128, (b) with seed pixel (58, 73) for the Lenna image of size 256×256, (c) with seed pixel (165, 43) for the Lenna image.

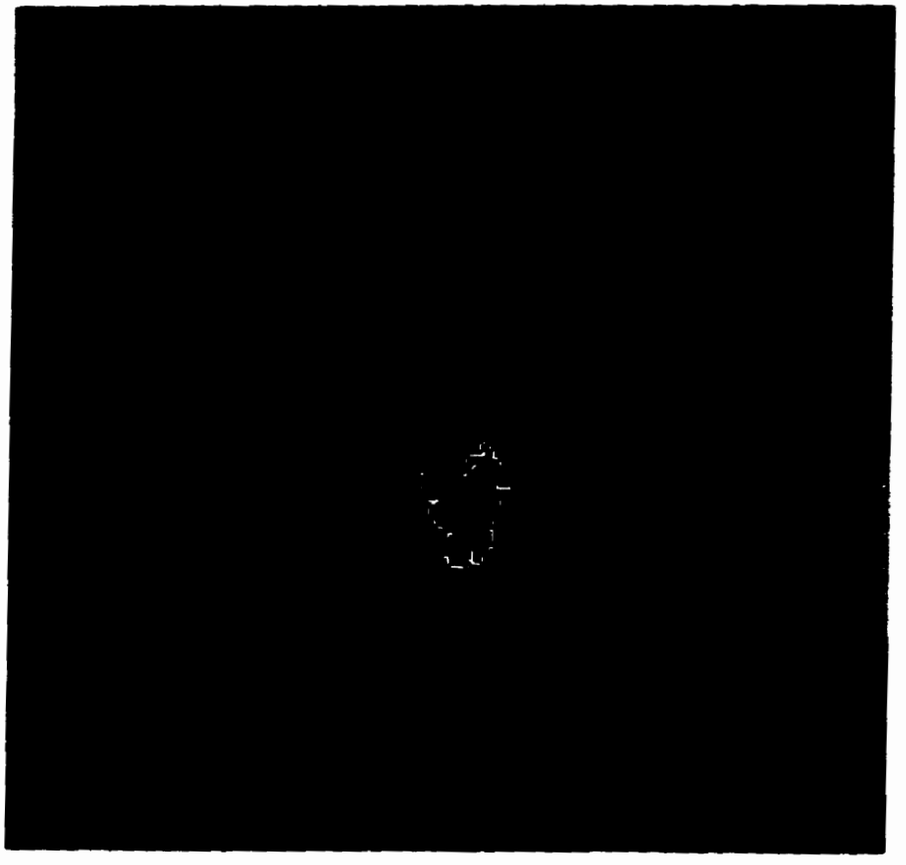

Figure 3.2. Overlapping ANs grown in the Lenna image.

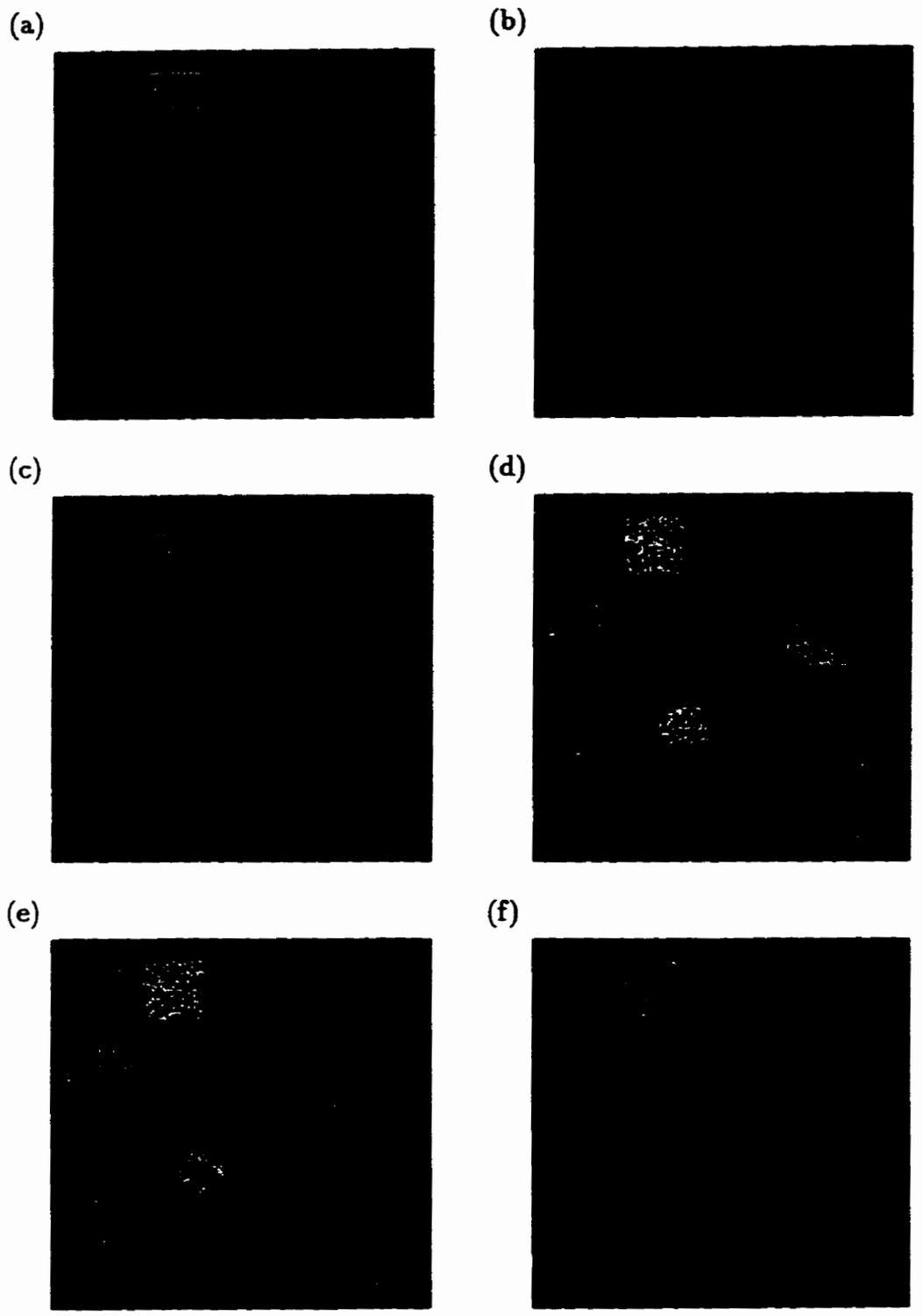

Figure 3.3. Original, noisy, and restored versions of the first synthesized image: (a) Original, (b) image with multiplicative noise, (c) image restored by the 3×3 mean filter, (d) image restored by the ARW LMS method, (e) image restored by the method of Kuan et al., (f) image restored by the AN method after 4 iterations.

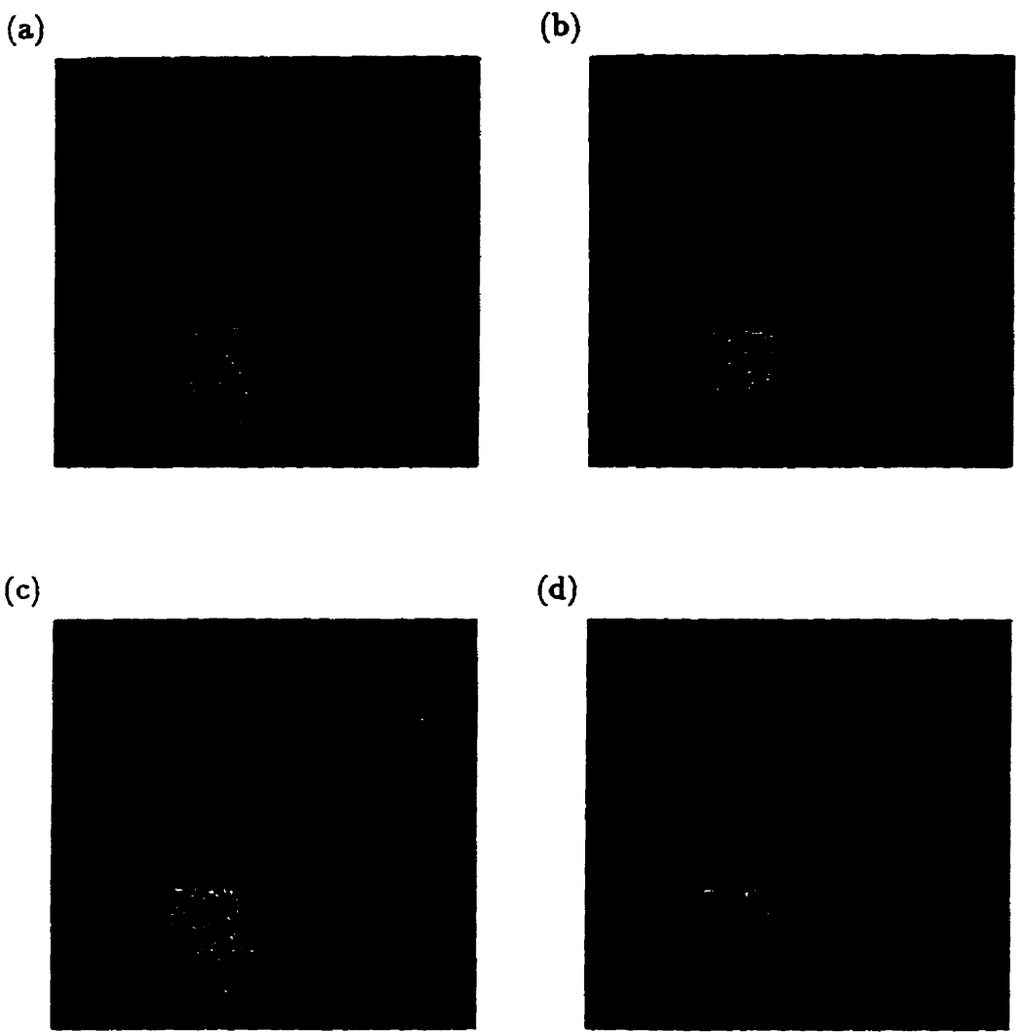

Figure 3.4. Original, noisy, and restored versions of the second synthesized image: (a) Original, (b) image with multiplicative noise, (c) image restored by the method of Kuan et al., (d) image restored by the AN method after 1 iteration.

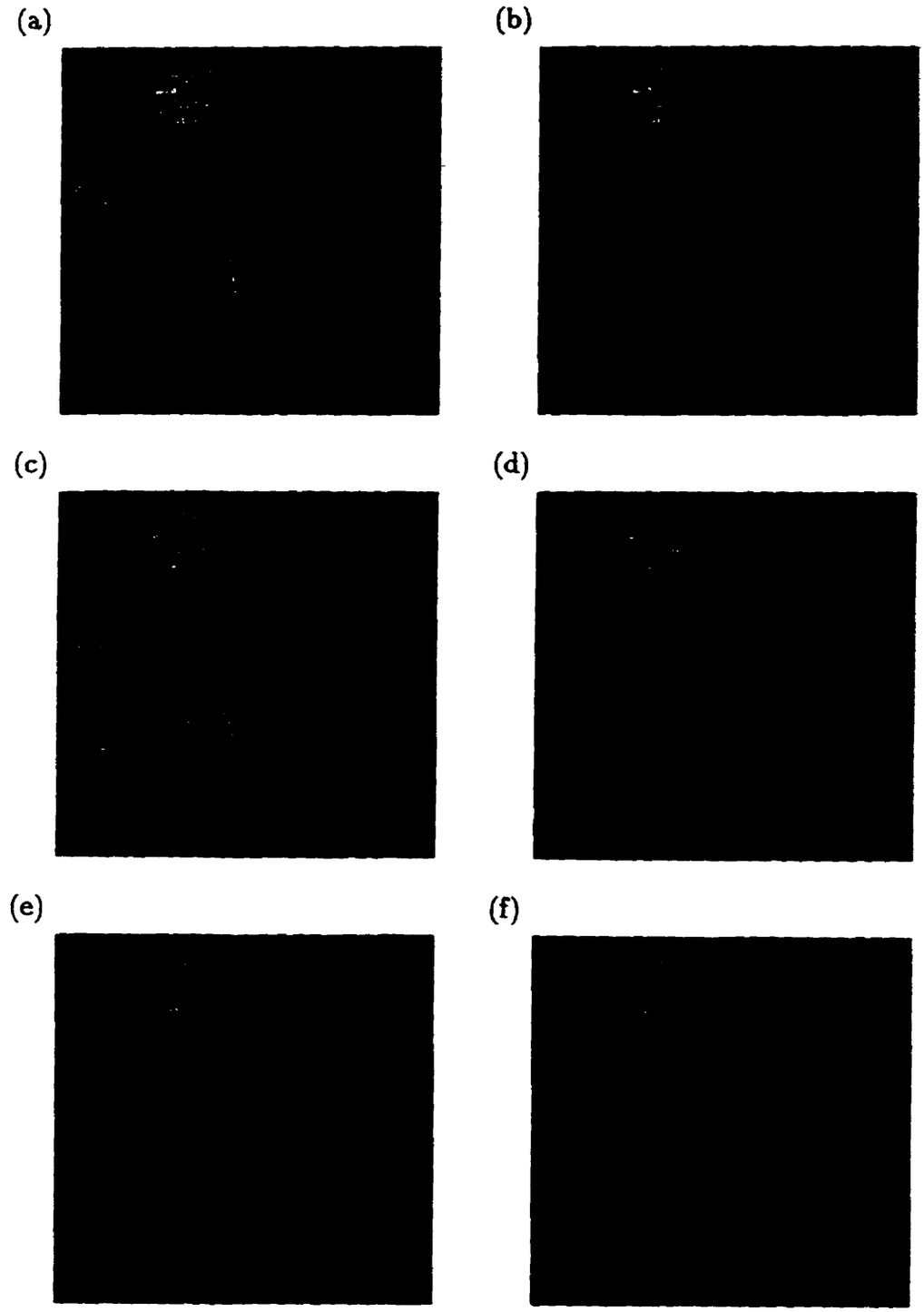

Figure 3.5. Restored images obtained after successive iteration with the AN method for the image in figure 3.3(b):
(a) after iteration 1, (b) after iteration 2, (c) after iteration 3, (d) after iteration 4, (e) after iteration 5, and (f) after iteration 6.

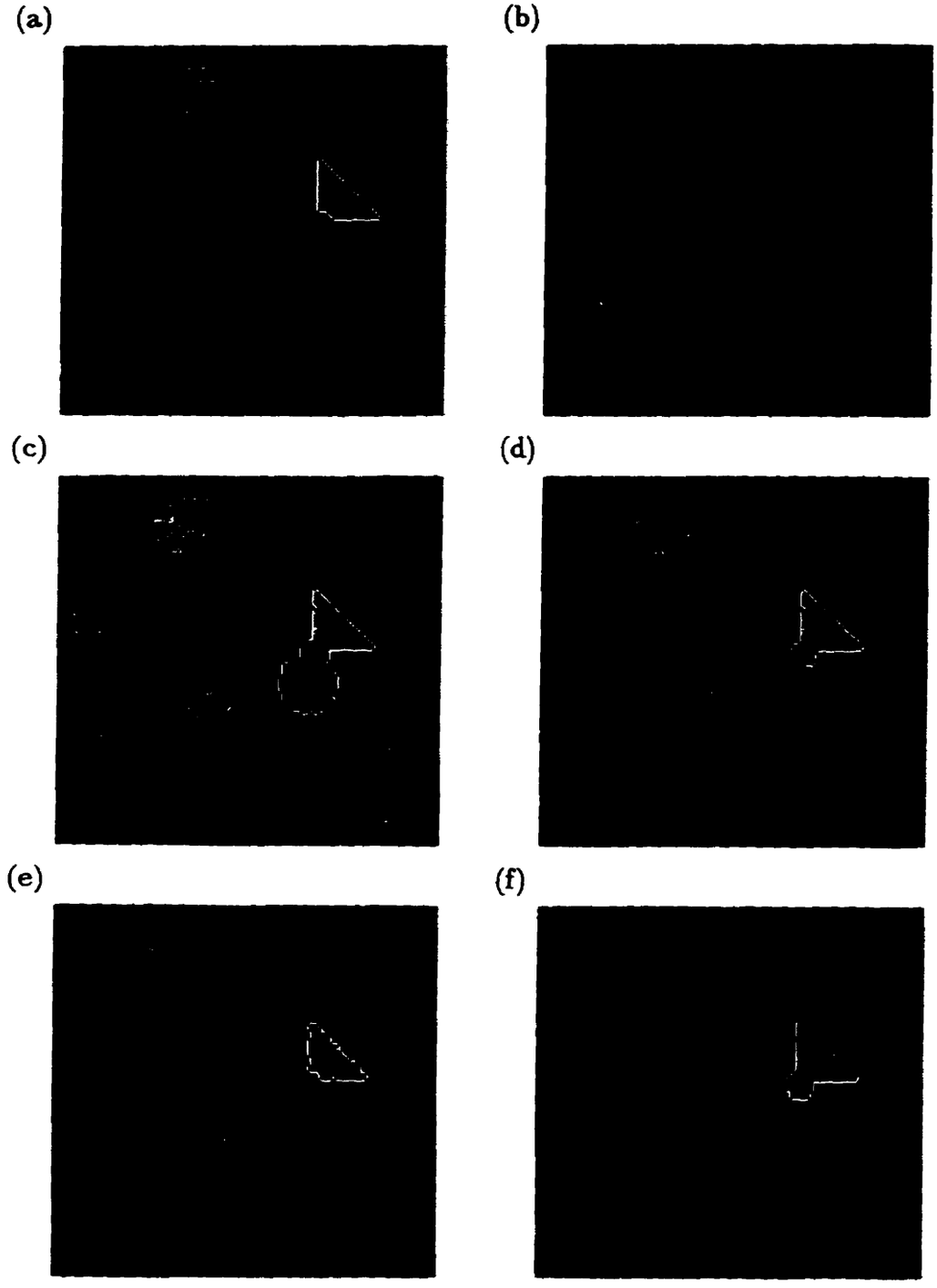

Figure 3.6. ANs grown with seed pixel (52, 94) for the original, noisy, and AN-restored versions of the first synthesized image in figure 3.3:
(a) region grown for the original image, (b) region grown for the noisy image,
(c) region grown for the image after iteration 1, (d) region grown for the image after iteration 3, (e) region grown for the image after iteration 4, (f) region grown for the image after iteration 5.

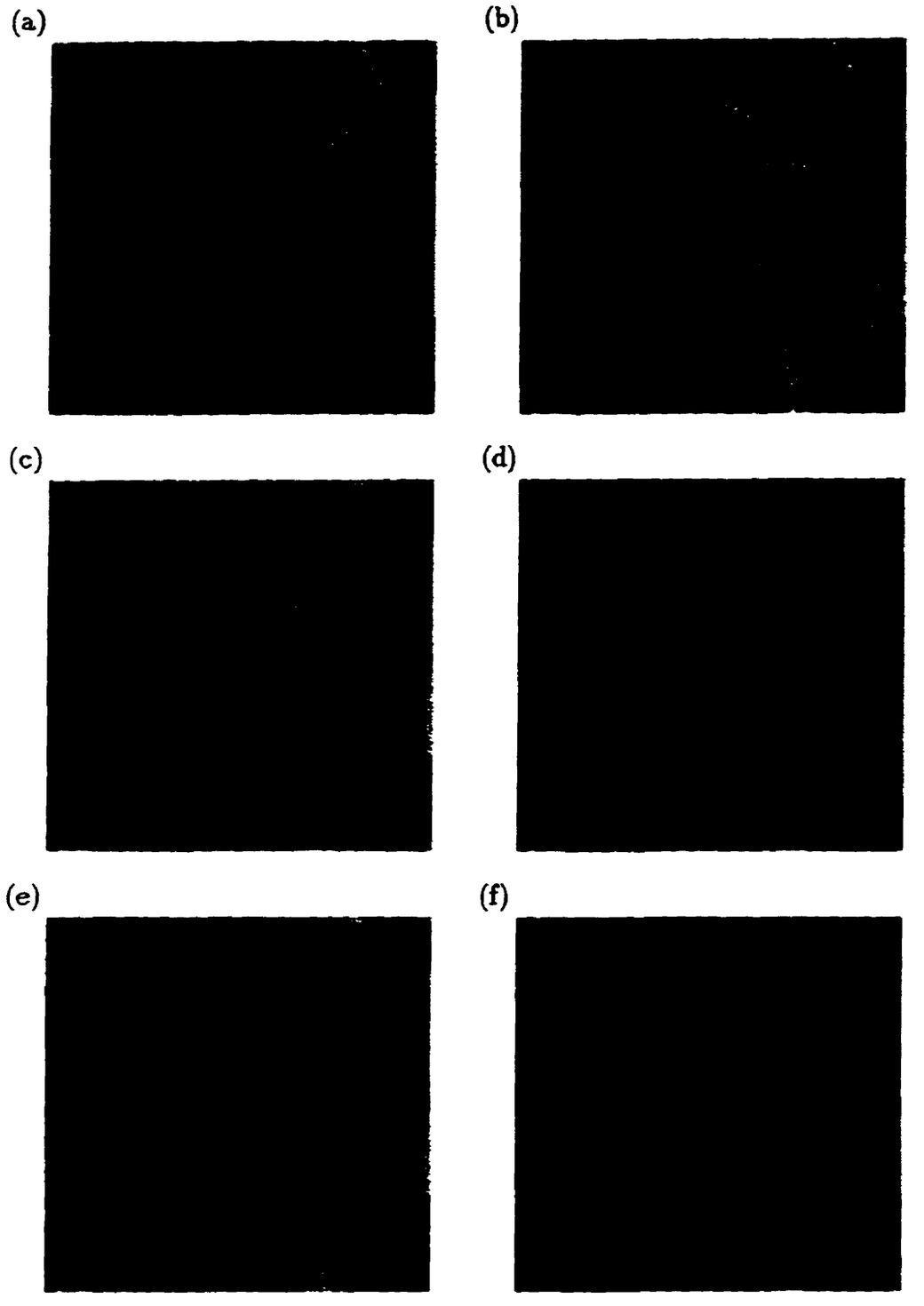

Figure 3.7. Original, noisy, and restored versions of the Lenna image:
(a) Original, (b) image with multiplicative noise, (c) image restored by the 3×3 median filter, (d) image restored by the ATD LMS method, (e) image restored by the method of Kuan et al., (f) image restored by the AN method after 3 iterations.

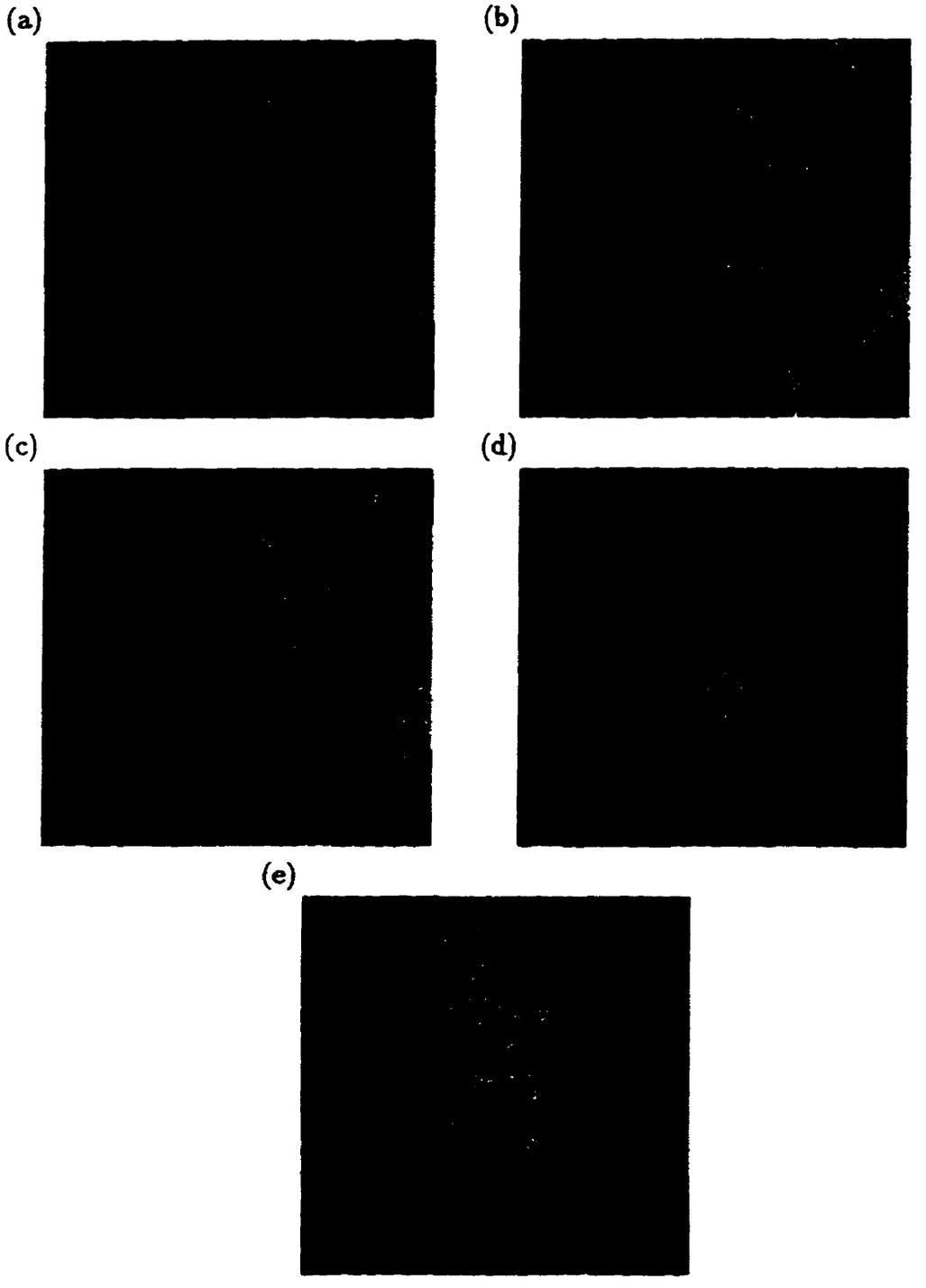

Figure 3.8. ANs grown with seed pixel (153, 135) for the original, noisy, and AN-restored versions of the Lenna image in figure 3.7:
(a) region grown for the original image, (b) region grown for the noisy image, (c) region grown for the image after iteration 1, (d) region grown for the image after iteration 2, (e) region grown for the image after iteration 3.

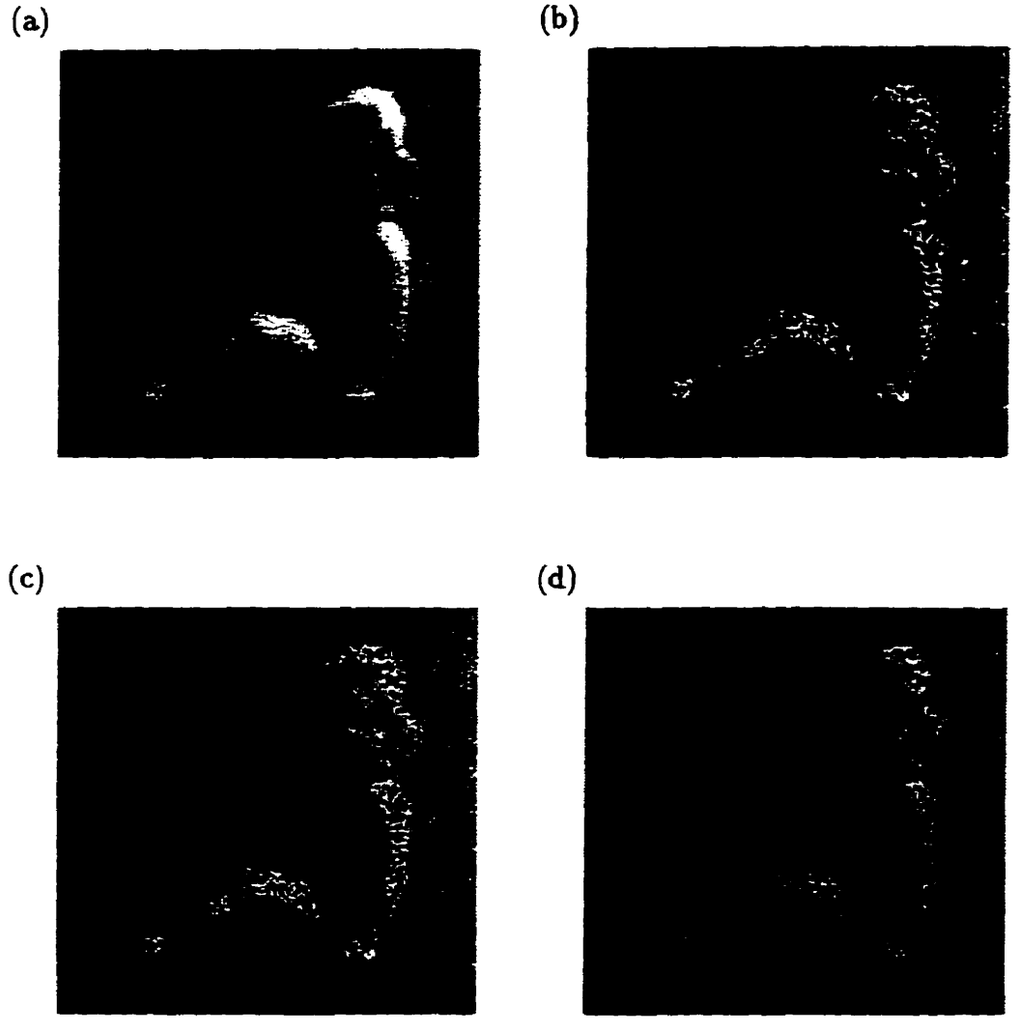

Figure 3.9. Original, noisy, and restored versions of the Sarah image:
(a) Original, (b) image with multiplicative noise, (c) image restored by the method of Kuan et al., (d) image restored by the AN method after 2 iterations.

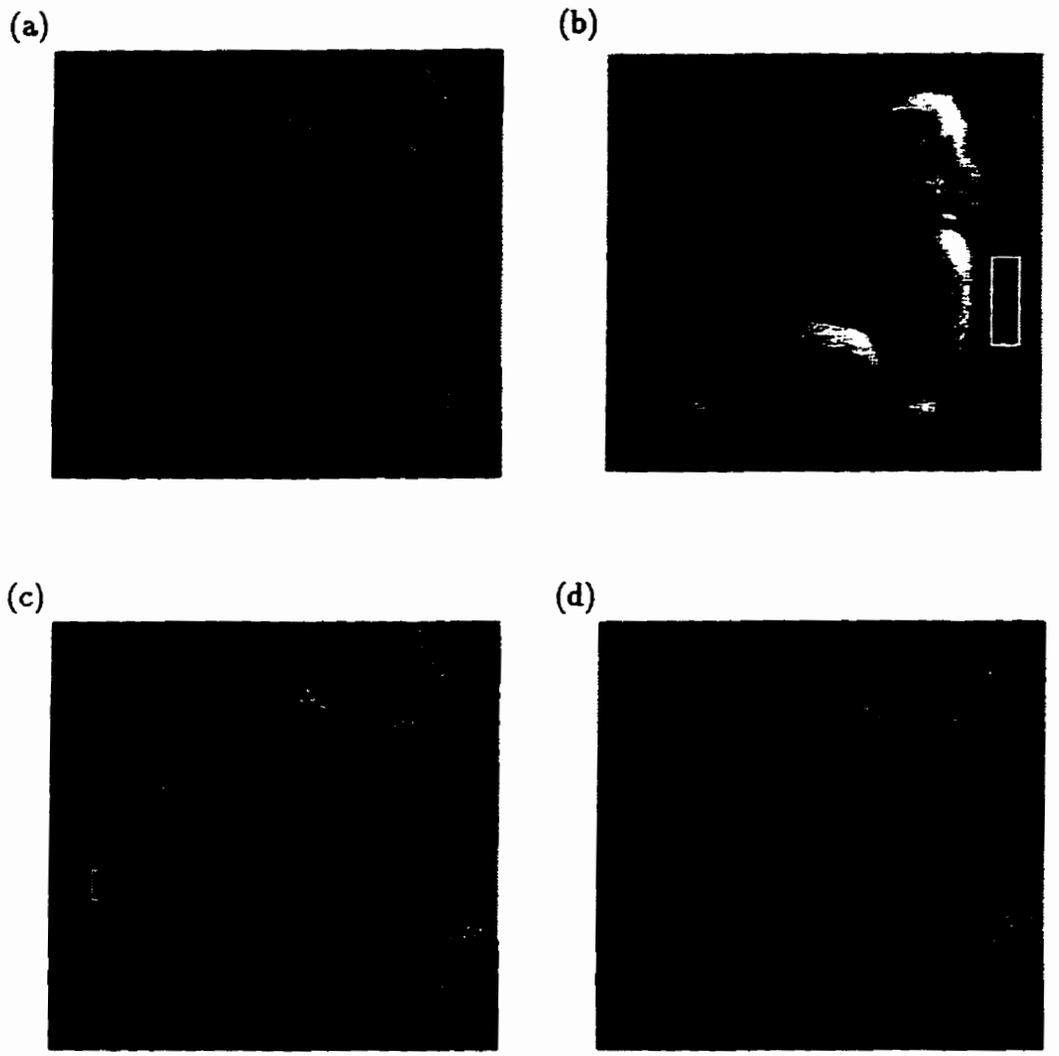

Figure 3.10. Rectangular areas for computing MSE in different regions of two natural images.

Images	MSE values for the synthesized test images	
	first image	second image
Noisy image	328.5	100.2
Image restored by the 3×3 mean filter	452.4	364.9
Image restored by the 3×3 median filter	342.1	251.3
Image restored by the ATD LMS algorithm	321.9	177.0
Image restored by the ARW LMS algorithm	369.1	313.3
Image restored by the ANNS algorithm	374.9	95.1
Image restored by the 3×3 filter of Kuan et al.	277.6	61.0
Image restored by the AN method (*)	128.5	34.8

Table 3.1: The MSE values of the noisy and restored versions of the two synthesized images in figure 3.3 and figure 3.4. (* After 4 iterations for the first image, and 1 iteration for the second image.)

Iteration	MSE
1	159.1
2	137.1
3	129.7
4	128.5
5	131.3
6	137.0
7	145.1

Table 3.2: The MSE values of restored result after each of the first seven iterations of the AN method for the first synthesized test image in figure 3.3.

Images	MSE values for the natural images	
	Lenna image	Sarah image
Noisy image	882.8	679.2
Image restored by the 3×3 mean filter	396.7	395.8
Image restored by the 3×3 median filter	296.9	388.3
Image restored by the ATD LMS algorithm	400.7	414.4
Image restored by the ARW LMS algorithm	876.3	675.2
Image restored by the ANNS algorithm	870.2	671.5
Image restored by the 3×3 filter of Kuan et al.	294.7	470.8
Image restored by the AN method (*)	219.2	331.7

Table 3.3: The MSE values of the noisy and restored versions of the two natural images in figure 3.7 and figure 3.9. (* After 3 iterations for the Lenna image and 2 iterations for the Sarah image.)

CHAPTER 4

REGION-BASED IMAGE EDGE PROFILE ACUTANCE

The sharpness of an image is related to the higher-frequency content of the image and to the edge information in the image. The mean-squared gradient is a reliable measure of edge sharpness, and has been used in the definition of the "acutance" of an edge or region of interest (ROI). In this chapter a new method of computing image edge profile acutance based on the mean-squared gradient along the normals to the boundary of an ROI is proposed.

4.1 Need for Measures of Image Sharpness

The process of capturing images of objects and scenes usually involves some degradation and loss of quality. The field of digital image processing provides a number of techniques to improve the quality of digital images by modifying image characteristics such as sharpness, contrast, dynamic range, and frequency content. However, judging the degree of improvement in perceptual quality provided by an operation is a rather difficult task as the quality of an image is a subjective concept dependent on various image characteristics, viewing conditions, and the visual system of the observer. Consequently, the need for objective correlates of the inherently subjective properties of image sharpness, crispness, quality, and perceptibility of details has been recognized for a long time (see Rangayyan and Elkadiki [38] for a review on this topic).

Higgins and Jones [39] discussed evaluation of sharpness of photographic im-

ages, with particular attention to the importance of gradients. They found that the maximum gradient or average gradient measures along knife-edge spread functions (KESFs) failed to correlate with sharpness, but that the mean-squared gradient across the KESFs, called acutance, indicated excellent correlation with subjective judgement of sharpness.

Wolfe and Eisen [40] stated that the sharpness of an image is a subjective concept as it is an impression made on the mind of an observer when viewing a picture. They observed that resolving power and sharpness do not have any psychophysical relationship, and found that the maximum and average gradients do not correlate well with the sharpness of the image. They stated that the variation of density across an edge is an obvious physical measurement to be investigated to obtain an objective correlate of sharpness.

Perrin [41] took the mean-square gradient measurement over many sections of the KESF, normalized the measured values with respect to the density difference across the knife edge, and called it acutance.

Crane [42] discussed the need for objective correlates of the subjective property of image sharpness or crispness; he remarked that resolving power is misleading, that the averaged squared gradient of edge profiles is dependable but cannot include the effects of all components in a photographic system (camera to viewer), and that spread functions and modulation transfer functions (MTFs) are not easy to comprehend, compare, or tabulate. He proposed a single numerical rating based on the areas under the MTF curves of all the systems in the chain from the camera to the viewer

called "system modulation transfer or SMT acutance" (SMTA). Later, Gendron [43] proposed a "cascaded modulation transfer or CMT" measure of acutance (CMTA) to rectify some deficiencies in SMTA. CMTA was used by Kriss to compare sharpness of imaging systems [44].

Higgins discussed various methods for analyzing photographic systems, including the effects of nonlinearity, line spread functions (LSFs), MTFs, granularity, and sharpness [45]. He also discussed quality criteria as related to objective or subjective tone reproduction, sharpness, and graininess, and recommended that MTF-based acutance measures are good when no graininess is present; signal-to-noise ratio (SNR) based measures were found to be better otherwise [46].

The concept of image sharpness or acutance has the potential to serve as a local measure of image quality or the perceptibility of a region or feature of interest. This has immense application in various fields, such as medical imaging, where one may obtain an array of images of the same patient (or phantom) using different imaging systems. The radiologist or medical physicist would be interested in evaluating which system or set of parameters provides an image of a specific object, such as a tumor, that can be perceived most accurately. Consequently, intensive research has been directed towards finding a quantitative measure of sharpness of an object or region of interest (ROI) (see Rangayyan and Elkadiki [38] for a review).

4.2 Methods for Computation of Edge Profile Acutance

The acutance measure A, proposed by Higgins and Jones [39] is given by the formula

$$A = \frac{1}{f(b) - f(a)} \int_a^b \left(\frac{df}{dx}\right)^2 dx, \tag{4.1}$$

where $f(x)$ is a section across the edge image (or KESF), and a and b are the edge start and end points, respectively. $(b-a)$ is related to the resolution of the edge, and $[f(b) - f(a)]$ is related to the contrast of the edge (see Hall [47]).

Rangayyan and Elkadiki [38] proposed a measure of mean-squared gradient computed across and around the contour of an ROI and called it "a region-based measure of image edge profile acutance (IEPA)". They used a region growing method (Morrow et al. [35]) for finding the boundary of the region. The method starts with a seed pixel within the ROI. A region is grown by aggregating 4-connected pixels which meet a pre-specified tolerance t about the seed pixel's gray level, defined as

$$|p(k,l) - p(i,j)| \leq t, \tag{4.2}$$

where $p(i,j)$ is the gray level of the seed pixel and $p(k,l)$ is the gray level at a connected pixel (k,l). The region growing process stops when no 4-connected pixel within the specified gray level tolerance can be found. When the region growing process is completed, the outermost layer of pixels of the region gives the region's external boundary.

Once the boundary is identified, the next task is to find the normals at all positions on the boundary. Rangayyan and Elkadiki [38] suggested consideration of three

boundary pixels at a time – the current, next, and previous – to find the normal to the boundary at the current pixel. The algorithm selects a set of nine pixels that approximate the normal at each pixel on the boundary by comparing the relative positions of the three boundary pixels selected.

A new method to determine the normals has been suggested by El-Faramawy et al. [48]. Instead of taking only three pixels on the boundary at a time to approximate the normals, they fitted a polygon to the ROI boundary, with the number of sides being dependent upon the ROI shape complexity. A linear equation is then available for each of the sides of the polygon, from which the equation for the normal to each side can be found easily. Using the equations of the normals, the pixels along the normals at each boundary pixel can be obtained. The details of the polygonal approximation method are provided in a paper by Ventura and Chen [49].

Rangayyan and Elkadiki [38] used four foreground pixels inside the region and four background pixels outside the region to define the normal. In the modified version proposed by El-Faramawy et al. [48], the number of pixels taken along each normal is variable, taking into consideration edge thickness and the available number of normal pixels. The edge pixel itself is not used in the computation. The following equation is then used to calculate the gradient at the boundary point under consideration (indexed j):

$$\bar{m}(j) = \frac{1}{N} \sum_{i=1}^{N} \frac{f(i) - b(i)}{2i}, \tag{4.3}$$

where N is the number of pixels taken along the normal, and $f(i)$ and $b(i)$ are the foreground and background pixels, respectively (see figure 4.1 for details on the index

i).

The procedure is repeated at all edge pixels (i.e. all pixels on the boundary of the ROI). After all the normal derivatives are calculated, the root mean squared (RMS) gradient is calculated over all pixels on the ROI boundary. The RMS value is then normalized by the maximum possible RMS derivative. The expression for IEPA is given by

$$\bar{A} = \frac{1}{d_{max}} \left[\frac{1}{B} \sum_{j=1}^{B} \bar{m}^2(j) \right]^{\frac{1}{2}}, \tag{4.4}$$

where $\bar{A}$ is the IEPA, $\bar{m}(j)$ is the averaged derivative at a particular boundary pixel j, B is the number of boundary pixels, and d_{max} is the maximum possible averaged derivative. In the paper by Rangayyan and Elkadiki [38], d_{max} was calculated to be 132.8125, assuming 8-bit digitization. In the modification suggested by El-Faramawy et al. [48], the value of d_{max} varies, depending upon the number of points taken along each normal. Acutance is a dimensionless quantity.

Olabarriaga and Rangayyan [50] explored the effectiveness of the IEPA measure in analyzing relative sharpness of different images affected by blur and noise. They obtained the subjective ranking of a set of test images and compared the results with the ranking according to the acutance values of the images. They found that trends of IEPA agree well with subjective ranking of sharpness of an ROI.

4.3 Continuous-gradient-based Image Edge Profile Acutance

In this section, a modification to the formula for computing the gradient across the edge pixel is suggested. The computation of acutance from the gradients is also

modified. The gradient is computed continuously instead of being computed using differences between corresponding pixels across the edge [38, 48].

For an image with digitized, finite pixels, a continuous derivative operation cannot be performed in the true sense – the normalized difference value between adjacent pixels can be calculated only as an approximation to the continuous derivative. The difference is normalized in order to take into account the varying distance between two adjacent pixels. In an 8-connected neighborhood, the four pixels at the corners are $\sqrt{2}$ distance units apart from the central pixel under consideration; the corresponding distance to the other four neighboring pixels is one unit. The gradient or derivative at the pixel i is computed as

$$d_i = \frac{n(i) - n(i+1)}{dist_i}, \tag{4.5}$$

where d_i is the derivative at the i'th pixel, and $n(i)$, $i = 1, 2, ..., N$, are the foreground and background pixels along the normal indexed successively (see figure 4.1). $dist_i$ is the distance between the i'th and $(i+1)$'th pixel, which is either 1 or $\sqrt{2}$ as discussed earlier.

After the gradient is calculated, the local acutance at the j'th boundary pixel is computed as

$$A_j = \left| \frac{1}{n(1) - n(N)} \right| \sum_{i=1}^{N-1} {d_i}^2, \tag{4.6}$$

where $n(N)$ and $n(1)$ are the pixel values of the N'th and the first pixel along the normal. The edge pixel is used in the computation, contrary to the previous methods [38, 48].

The local acutance value is then normalized by the maximum possible acutance value at point j, which is

$$A_{max_j} = \sum_{i=1}^{N-1} 255^2, \tag{4.7}$$

for 8-bit quantization.

A_j in equation (4.6) is maximum when the numerator is maximum and the denominator is minimum. The numerator is maximum when each pair of pixels has unit distance and a pixel value difference of 255. It is assumed that the background of an object does not include another object, and that the denominator can have a minimum value of 1.

Equations (4.6) and (4.7) are applied at all edge pixels. After all normalized local acutance values have been calculated, the final acutance is computed by averaging the normalized local acutance values over all pixels on the boundary as

$$A = \frac{1}{B}\left[\sum_{j=1}^{B} \frac{A_j}{A_{max_j}}\right], \tag{4.8}$$

where A is the final acutance value and B is the number of pixels on the boundary. Acutance A above is a dimensionless quantity similar to the one defined by Higgins and Jones [39].

The most important difference between the proposed algorithm and the previous algorithms [38, 48] is in the definition of the gradient. According to the original definition given by Higgins and Jones [39], acutance or edge sharpness is related to the mean-squared gradient of the edge. The algorithms of Rangayyan and Elkadiki [38] and El-Faramawy et al. [48] used the RMS value of averaged differences.

Secondly, the previous method of taking the differences between corresponding pixels across the edge is dependent on the knowledge of the exact position of the edge pixels. The exact position of edge pixels cannot be determined for most natural images. In real situations one can identify only a region containing the edge instead of finding the exact edge-pixel. Approximating the derivative by taking differences across the edge pixel is arbitrary as well. Theoretically, the gradient at any point of a discrete function is approximated by the normalized difference with respect to the previous point. The edge function of a digital image is a discrete function and hence the gradient of the edge should be calculated using the method described in the proposed algorithm based on differences between successive pixels. The method proposed in this section is independent of the knowledge of the exact edge pixel. Therefore the proposed algorithm can be taken as the formal definition of acutance for digital images as it agrees with the original definition of acutance given by Higgins and Jones [39].

4.4 Evaluation with Test Images

The modified algorithm was evaluated with two test images (used by Rangayyan and Elkadiki [38]). The first image is an image of the letter R (figure 4.2(a)) which was produced by digitizing a printout of the letter R to a 256×256 array with 256 gray levels. The R image was corrupted by adding uniformly-distributed random noise in the range of +50 to −50 (figure 4.2(b)) and blurred using a 3×3 mean lowpass filter. Figures 4.2(c) and 4.2(d) show the blurred versions of the R image after one

pass and four pass of the mean lowpass filter, respectively. The original R image was converted to a bi-level (gray values 0 and 255) image (figure 4.2(e)) to find the maximum achievable acutance by the proposed method.

The second test image is a dragonfly image (figure 4.3(a)) which was obtained by digitizing a natural image. The image is a 256×256 image with gray levels varying from 0 to 255. The image was corrupted by adding uniformly-distributed noise in the range of +50 to −50 (figure 4.3(b)). Blurred versions of the image were acquired by adjusting the focus of the digitizing camera. Figures 4.3(c) and 4.3(d) show the blurred dragonfly images with level 1 and level 2 blurring, respectively. The original and blurred dragonfly images were enhanced by the 3×3 subtracting Laplacian operator [34] to verify if acutance values are higher for the enhanced images. All the processed and unprocessed versions of the image were histogram equalized to permit direct comparison. Figure 4.3(e) shows the original image after histogram equalization, and figure 4.3(f) shows the original image after subtracting Laplacian and histogram equalization operations.

For the sake of consistency, the same ROI boundary derived from the original image was used for computing acutance for all the versions of each test image. Tables 4.1 and 4.2 list the acutance values for the test images using the method by Rangayyan and Elkadiki [38], the method by El-Faramawy et al. [48], and the method described in the previous section. From the results in the tables, it is seen that the acutance values computed by the proposed modified algorithm lie in a different range, but follow the same trend for different versions of the test images as exhibited by the

acutance values obtained by the other two methods: acutance decreases as sharpness decreases (with increased blurring). Histogram equalized images have increased acutance values, with the versions after subtracting Laplacian and histogram equalization operations having larger acutance values than the original and the one after histogram equalization alone. The modified method, however, is more sensitive to noise, and acutance increases slightly with the addition of noise.

The magnitude of the acutance computed by the proposed method is small, which may be due to the over-restrictive nature of the maximum value used for normalization. The algorithm takes the maximum pixel value difference between two adjacent pixels as 255 (assuming 8-bit digitization). However, within an ROI, the differences between two adjacent pixels both belonging to the ROI (and quite likely the background as well) cannot be 255 because of the way the pixels are aggregated to form the ROI. The maximum value of acutance, which occurs for a bi-level ROI, is thus far less than 1.

4.5 Summary

We have proposed a modified method for computing the acutance of an ROI: the proposed algorithm is an extension of the work by Rangayyan and Elkadiki [38] and El-Faramawy et al. [48]. The method uses the conventional difference operator instead of a variable-step difference operator. The proposed algorithm can be taken as the discrete version of the original mean squared gradient definition of acutance as a continuous integral of the edge spread derivative proposed by Higgins and Jones [39].

The validity of the algorithm is demonstrated by the fact that the measure decreases with blurring and increases with sharpening. Further tests need to be conducted in order to establish the relation between the acutance values proposed by the new method and subjective ranking [50].

IEPA gives a quantitative measurement of the gradients across boundaries of an ROI, which is very important for visual perception. Given the improved definition of IEPA in this chapter, image enhancement algorithms can be designed specifically to increase IEPA and hence improve the perceptibility of an ROI. In the next chapter, we will propose 1D enhancement operators for application along the normals of an ROI to improve edge sharpness, acutance, and hence perceptibility.

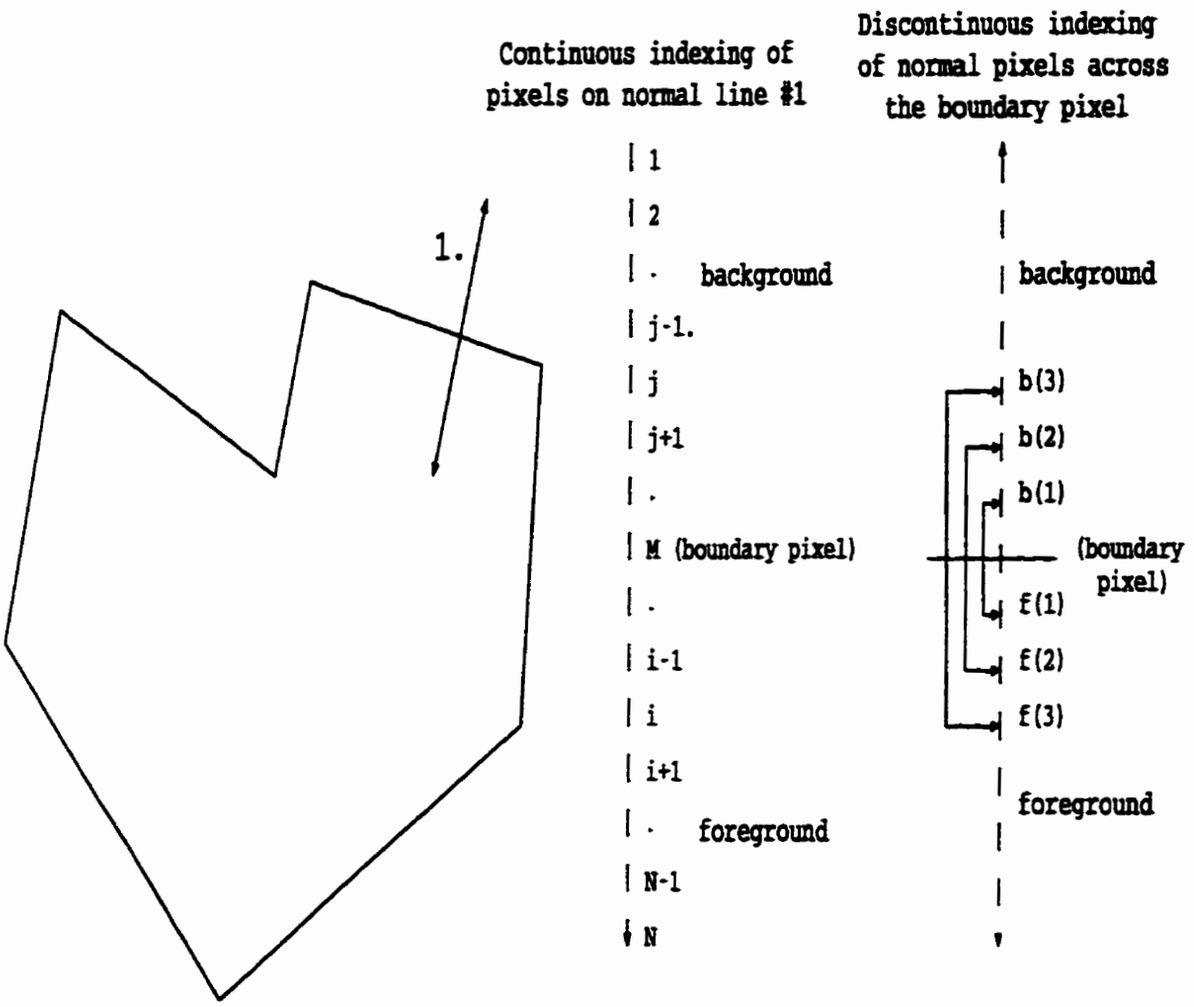

Figure 4.1. Indexing of normal pixels inside and outside an ROI.

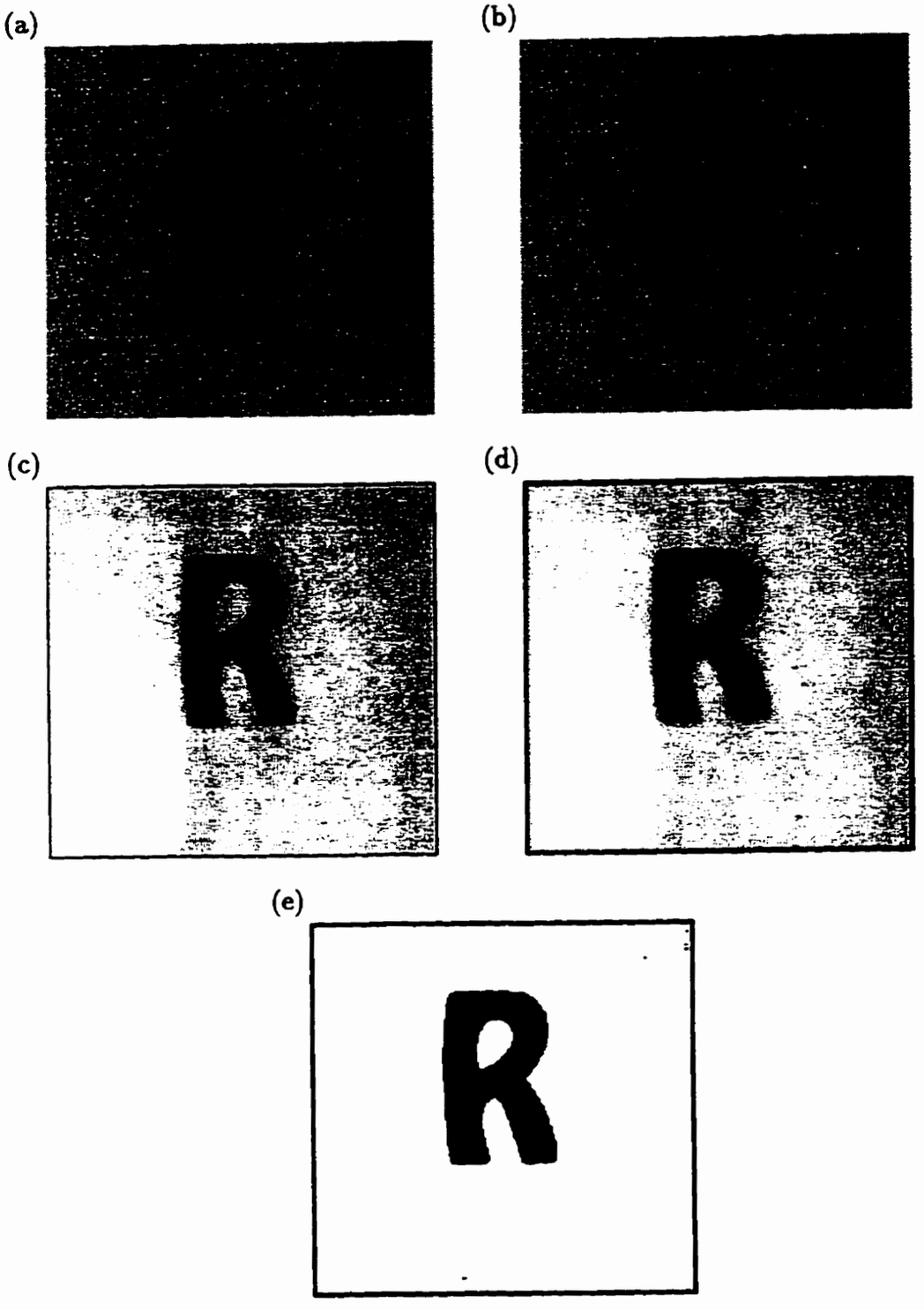

Figure 4.2. Original, noisy, blurred, and bi-level versions of the R image:
(a) Original, (b) image with noise, (c) image blurred by one pass of the 3×3 mean filter, (d) image blurred by four passes of the 3×3 mean filter, (e) bi-level image.

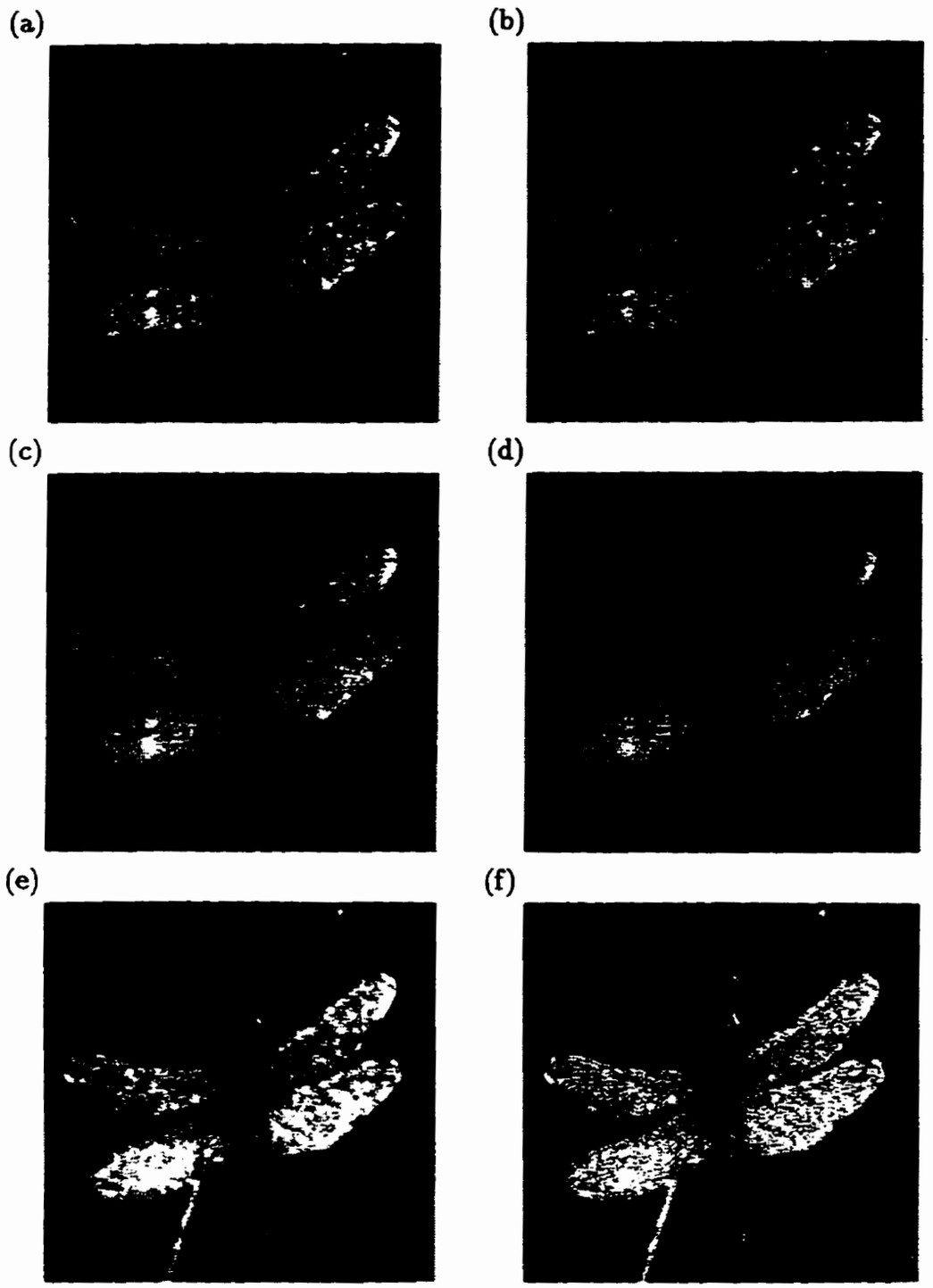

Figure 4.3. Original, noisy, blurred and enhanced versions of the dragonfly image: (a) Original, (b) image with noise, (c) image with level 1 blurring by lens misfocus, (d) image with level 2 blurring by lens misfocus, (e) original image after histogram equalization, (f) original image after subtracting Laplacian and histogram equalization operations.

Images	IEP acutance values by		
	the method by Rangayyan and Elkadiki	the method by El-Faramawy et al.	the proposed method ($\times$ 100)
Original R	0.410	0.587	0.205
Original + noise	0.395	0.562	0.232
Blurred once	0.373	0.581	0.182
Blurred twice	0.339	0.442	0.168
Blurred thrice	0.313	0.375	0.158
Blurred four times	0.278	0.245	0.152
bi-level	1.000	1.000	0.443

Table 4.1: Image edge profile (IEP) acutance values of the original, noisy, blurred, and bi-level versions of the R image obtained by using the method by Rangayyan and Elkadiki, the method by El-Faramawy et al., and the proposed method.

Images	IEP acutance values by		
	the method by Rangayyan and Elkadiki	the method by El-Faramawy et al.	the proposed method ($\times$ 100)
Original dragonfly	0.331	0.462	0.362
Original + noise	0.311	0.452	0.365
Blur level one	0.271	0.431	0.213
Blur level two	0.213	0.438	0.195
Original histogram equalized	0.415	0.654	0.682
Original after subtracting Laplacian and histogram equalization	0.485	0.650	0.726
Blur level one histogram equalized	0.357	0.488	0.320
Blur level one after subtracting Laplacian and histogram equalization	0.397	0.522	0.591
Blur level two histogram equalized	0.294	0.414	0.275
Blur level two after subtracting Laplacian and histogram equalization	0.313	0.507	0.516

Table 4.2: Image edge profile acutance values of the original, noisy, blurred, and enhanced versions of the dragonfly image obtained by using the method by Rangayyan and Elkadiki, the method by El-Faramawy et al., and the proposed method.

CHAPTER 5

REGION-BASED EDGE ENHANCEMENT

As acutance is correlated with image sharpness (Olabarriaga and Rangayyan [50]), one possible approach to image enhancement is to apply enhancement techniques in such a way as to increase the acutance of the ROI. Then, we may expect the perceived sharpness of the ROI to be increased as a result. A new image sharpening method designed on the basis of acutance is proposed in this chapter. In this method, one-dimensional operators are applied to sets of pixels along the normals at each boundary pixel of an ROI.

5.1 Edge Enhancement

As discussed in the previous chapter, the concept of edge sharpness of an image is particularly important in the visual perception of an image. Grossberg [51] stated that an important early stage of human vision involves the calculation of an edge map. He also proposed that the perception of brightness is controlled by a diffusion process in which the perceived contrast of the edges acts as an insulation strength that partially blocks the diffusion. Attenave [52] proposed that human beings are able to recognize objects starting from a very crude outline, and that edge detection may be the most important method of feature extraction in low-level vision.

The psychophysical importance of edge sharpness reflects itself in recent adaptive image contrast enhancement techniques. Some of the current adaptive contrast en-

hancement techniques have been developed with a view to take explicit account of local image structures (Morrow et al. [35]). Perona and Malik [54], working in the context of edge detection and the theory of scale-space anisotropic diffusion, developed a way of producing truly variable contextual regions for contrast enhancement in a manner very much like the description of the human visual system given by Grossberg [52]. Beghdadi and Le Negrate [55] used a modified contrast definition based on the detection of edges within contextual regions. Cromartie and Pizer [56] discussed the importance of edges in contrast perception and outlined the development of two adaptive contrast enhancement methods which take into account edge information in the image.

Many methods are available to increase edge sharpness; they may be classified into two broad categories: fixed-neighborhood methods such as subtracting Laplacian and unsharp masking (see Gonzalez and Woods [34]), and adaptive image sharpening methods. Some of the adaptive image sharpening and edge enhancement methods are reviewed below.

Marr [57] and Hildreth [58] relied on the knowledge that the human visual system uses edge detection techniques in the early stages of visual processing. They tried to understand and model this process, and on the basis of neurophysical studies developed a computational model for edge detection. Van Vliet et al. [59] developed an adaptive edge detection method based upon the detection of zero crossings in the output image of a nonlinear Laplacian filter adaptively oriented to the direction of the local gradient. Moron [60] presented a gradient-determined gray level morpho-

logical opening procedure for edge enhancement. Saint-Marc et al. [61] proposed a nonlinear filtering method for discontinuity-preserving smoothing; their methods were able to achieve edge sharpening after a few iterations. However, as the method was not primarily designed for sharpening the image, the enhancement achieved was not prominent.

In section 5.2 we will discuss a region-based method for edge enhancement of bi-level images. Though the method is intended to increase the edge-sharpness in bi-level images, the concept can be extended to sharpen gray level images.

5.2 Region-based Edge Enhancement

As acutance is related to the sharpness of the image, the image could be enhanced by using operators which increase the acutance of the ROI. Acutance is calculated using pixels along the normal at each boundary point. The proposed enhancement algorithm applies 1D operators on the normal pixels. The operators are derived using the following process.

When an image is blurred, the gradient of the edge is decreased, which is confirmed by a reduced acutance value. The gradient of the edge becomes lower as the differences between the values of pixels belonging to the foreground (object) and the background become smaller. This implies that the values of the background (or the foreground) pixels get farther from the average background (or the average foreground) value.

The gradient value of a blurred edge may be increased by processing the edge pixels so that they become closer to the foreground (or the background) value. There are

two difficulties associated with this approach: The first difficulty lies in identifying the edge pixels; in real images, the edge pixels are not defined well. The second difficulty is that a priori knowledge of the image is not available in most cases, and hence it may not be possible to ascertain the amount by which the pixel values need to be changed. The proposed algorithm reduces the gray level differences between the edge pixels and the foreground (or the background) pixels without assuming any prior knowledge of the edge pixels or their values before blurring, as follows.

The normal pixels at each boundary point are found by the method proposed by El-Faramawy et al. [48] and summarized in chapter 4. The enhancement algorithm starts with the farthest normal pixel in the background and proceeds towards the ROI boundary along the normal, while applying an operator such that the processed normal pixel values get closer to the background value. The 1D operator used is

$$n(j) = 2n(j-1) - n(j+1),\ j = 2, 3, ..., M, \tag{5.1}$$

where n is the normal pixel array, j is the index of the pixel under consideration, and M is the index of the boundary pixel in the normal array (see figure 4.1). The operator in equation (5.1) applies more weight to the pixel closer to the background than to that closer to the boundary. The changed pixel value is successively used for processing subsequent pixels.

The operator is applied along the normal pixels at each ROI boundary pixel. Some pixels may be selected for processing more than once. There are two approaches to consider regarding multiple processing of a normal pixel. The first approach is to allow

several modifications to the same pixel and then to take the average of the processed values. The second approach is to process each pixel only once by using flags. We observed in our experiments that the second approach provides better performance than the first.

A problem associated with the operator in equation (5.1) is that false contours may appear in the processed image. As the operator is a 1D operator, it processes a pixel on the basis of its two neighbors only, instead of the 2D 4-connected or 8-connected neighborhood. As a result, the value of the processed pixel may change drastically after processing when compared to the unchanged neighborhood, resulting in false contours. To prevent this problem we add a restriction such that the difference between a pixel value before and after processing is less than a threshold value. If the processed pixel value changes by more than the threshold, then the algorithm retains the original value of the pixel and does not mark it as "processed", and the pixel is available for further processing. The value of the threshold is determined by trial and error.

The algorithm compares the relation between the j'th and the $(j-1)$'th pixel before and after processing. If the value of the j'th pixel was less (more) than the value of the $(j-1)$'th pixel before processing but becomes more (less) after processing, then the algorithm retains the original value of the pixel. The pixel is not marked as processed, and is available for further processing.

For processing normal pixels belonging to the foreground, the algorithm is the same as for processing the background pixels; however, the sense of differentiation

along of the normal array is in the opposite direction (see figure 4.1). The operator used for processing the foreground pixels is

$$n(j) = 2n(j+1) - n(j-1),\ j = N-1, N-2, ..., M+1, \tag{5.2}$$

where N is the number of pixels in the normal array and M is the boundary pixel index.

The operator in equation (5.2) applies more weight to the pixel which is closer to the foreground or ROI center than to the other pixel used in the differentiation operation. For maintaining the mutual relationship between neighboring pixels, the algorithm compares the j'th pixel with the $(j+1)$'th pixel.

5.3 Results

The image enhancement algorithm was tested on two synthesized images. The first image is a 256x256 synthesized image containing a uniform square of size 90x90 and gray level 128 on a uniform background of gray level 255 (figure 5.1(a)). The second image is a 512x512 bi-level image with various objects in the form of rectangles, circles, and triangles. The gray level value of the objects was 0, with the background being a constant of 255. The various objects were allowed to intersect, with the gray level of the intersection being 0. Each region is thus uniform (i.e. the second test image is piece-wise constant). Figure 5.2(a) shows the second test image. Both the images were blurred once by applying a 7×7 mean filter; the corresponding images are shown in figures 5.1(b) and 5.2(b), respectively.

The first test image was sharpened by 3×3 subtracting Laplacian, 3×3 unsharp

masking, and the proposed method. The pixel values in the processed images were linearly mapped to the range 0-255 for display. The conventional spatial domain sharpening operators (the subtracting Laplacian operator and the unsharp masking operator) did not produce any significant improvement in the images; further, they produced noticeable edge artifacts in the processed images. The different images in figure 5.1 illustrate the enhancement achieved by the proposed method and also by the conventional sharpening operators. Edge profiles for the original, blurred, and the processed images are shown in figure 5.3. The profiles confirm that the proposed method sharpens the image more than the conventional methods, and further that the edge artifact produced by the 3×3 operators is absent in the result of the proposed method.

The acutance values (computed by the proposed method described in chapter 4) of the original, blurred, and processed versions of the square image are listed in table 5.1. From the table it can be observed that the subtracting Laplacian operator increases the acutance value of the blurred image. The increase in acutance value due to the unsharp masking operator is less than that produced by the subtracting Laplacian operator. The proposed enhancement algorithm increases the acutance value by the largest extent.

The second test image was sharpened by applying the subtracting Laplacian operator and the proposed method to each of the five objects in the image. The subtracting Laplacian operator produced edge artifacts and did not produce good enhancement. On the other hand, the image was sharpened considerably by the proposed method.

Figure 5.2 shows the different versions of the second test image, and figure 5.4 shows representative edge profiles of one of the objects in the images in figure 5.2. The profiles show that the proposed method increases sharpness more than the subtracting Laplacian operator. However, figure 5.2(d) shows that some artifacts appear at the corners of the objects. Note also that the circular region has been sharpened to a lesser extent than the other regions.

The acutance values of the five regions in the four images in figure 5.2 are listed in table 5.2. The blurred regions have much less acutance values compared to their original values. The acutance values are slightly increased by the subtracting Laplacian. The proposed method increases the acutance values by a larger factor than the subtracting Laplacian.

5.4 Summary

We have suggested a method for increasing the sharpness of an image on the basis of its acutance property. The method has shown much better performance than conventional spatial operators (such as 3×3 subtracting Laplacian and unsharp masking operators) and frequency domain sharpening operators (e.g. Butterworth high-emphasis filter; results not shown here) when applied to test images. The proposed method has achieved the main objective of the work – that of enhancing edge sharpness without artifacts such as overshoot and undershoot (ringing).

Initial tests of the methods, as reported here, have been limited to bi-level, synthesized images. Thresholding the blurred image could be an effective way to remove the

effects of blurring in bi-level images. However, while thresholding restores the sharpness of the image, edges are often displaced in the enhanced image. The proposed enhancement algorithm maintains edges in almost the same positions as in the original image. Restoration filters such as the Wiener filter [34] require exact knowledge of the blurring function. The proposed method, on the other hand, works without any a priori knowledge of the blurring function or the original image.

The proposed method has some minor limitations as mentioned earlier. The problem of corner artifacts is due to difficulties in finding the normal pixels at corners. The boundary of a circular ROI cannot be very well approximated by a finite number of linear segments; thus the degree of enhancement is less for a circular ROI. These limitations need to be addressed in future work.

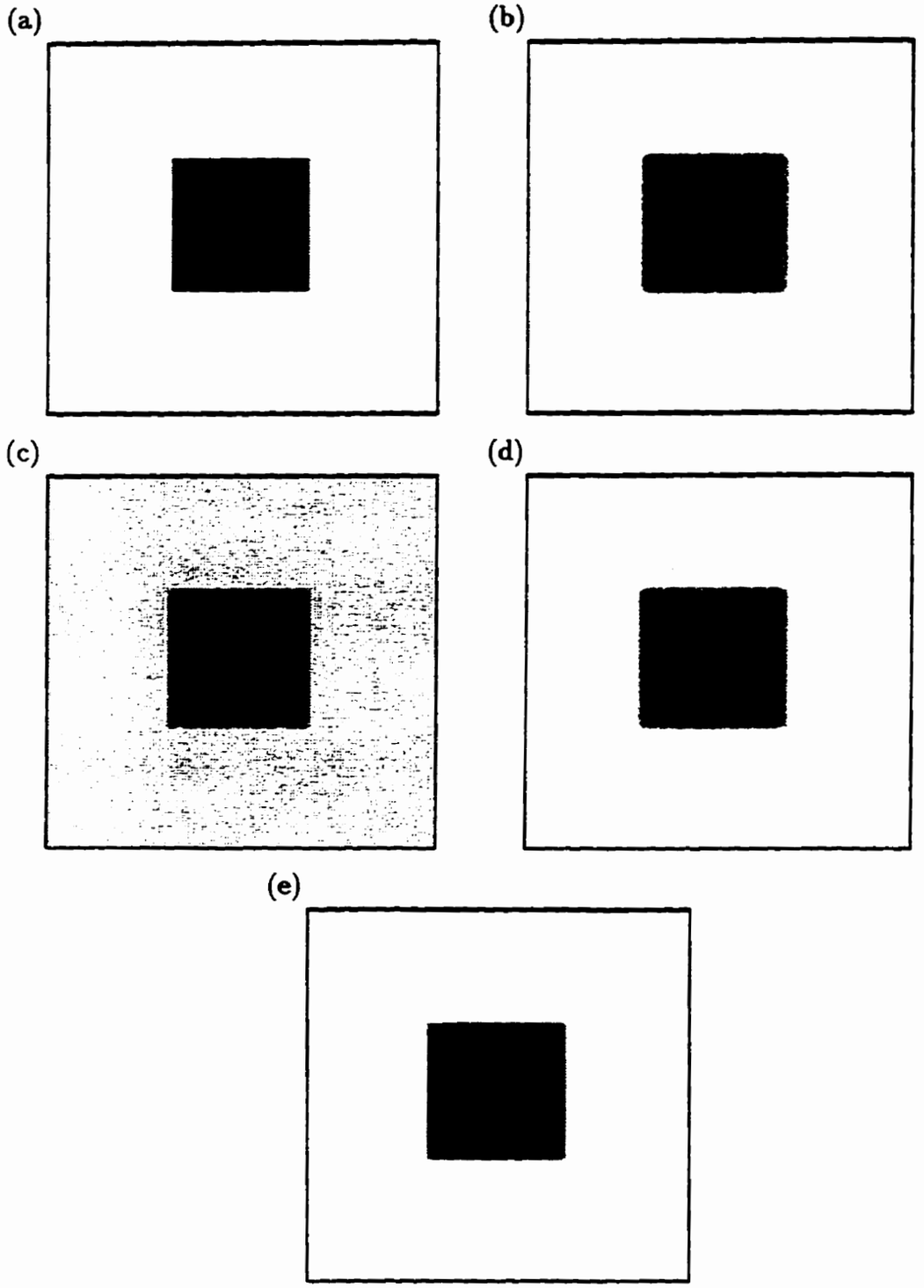

Figure 5.1. Original, blurred, and sharpened versions of the first test image: (a) original, (b) blurred, (c) enhanced by subtracting Laplacian, (d) enhanced by unsharp masking, (e) enhanced by the proposed method.

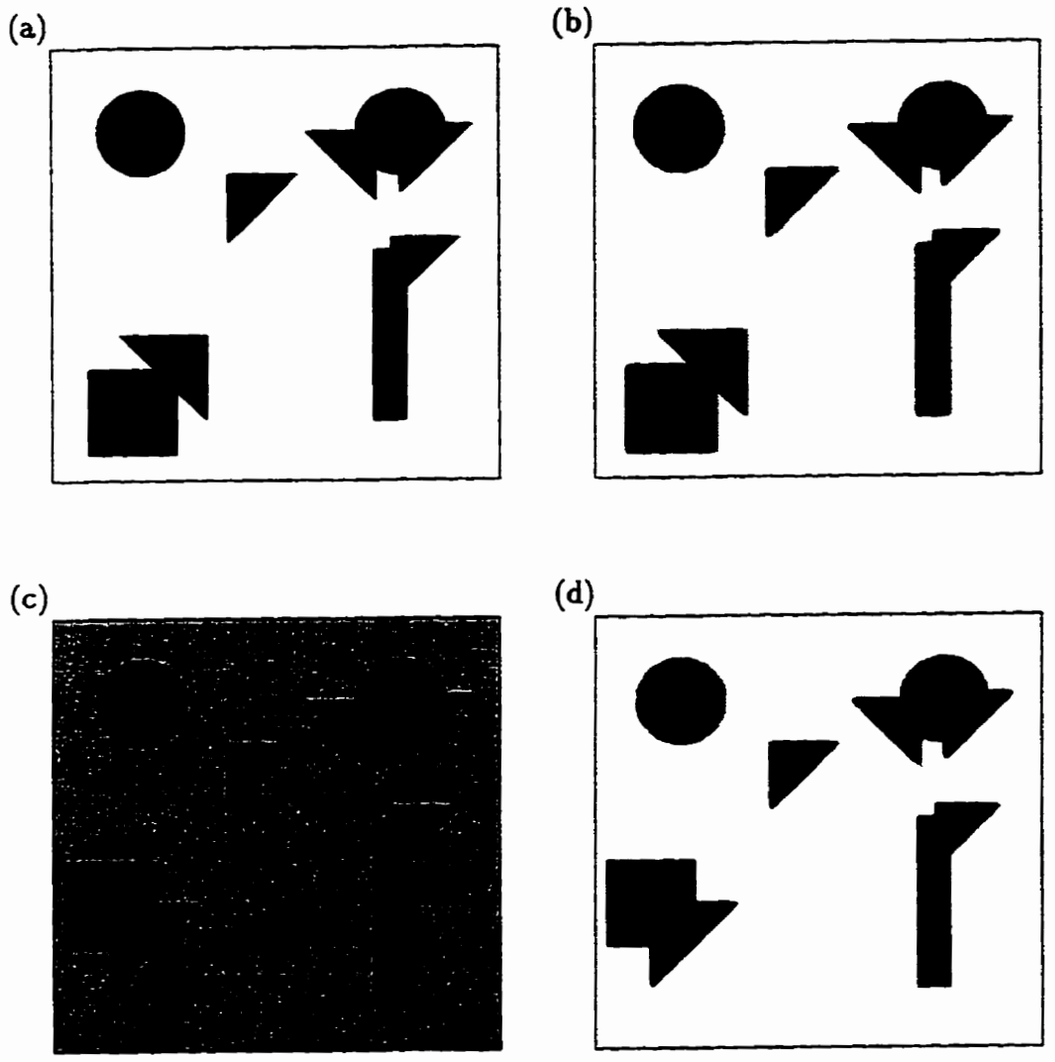

Figure 5.2. Original, blurred, and sharpened versions of the second test image: (a) original, (b) blurred, (c) enhanced by subtracting Laplacian, (d) enhanced by the proposed method.

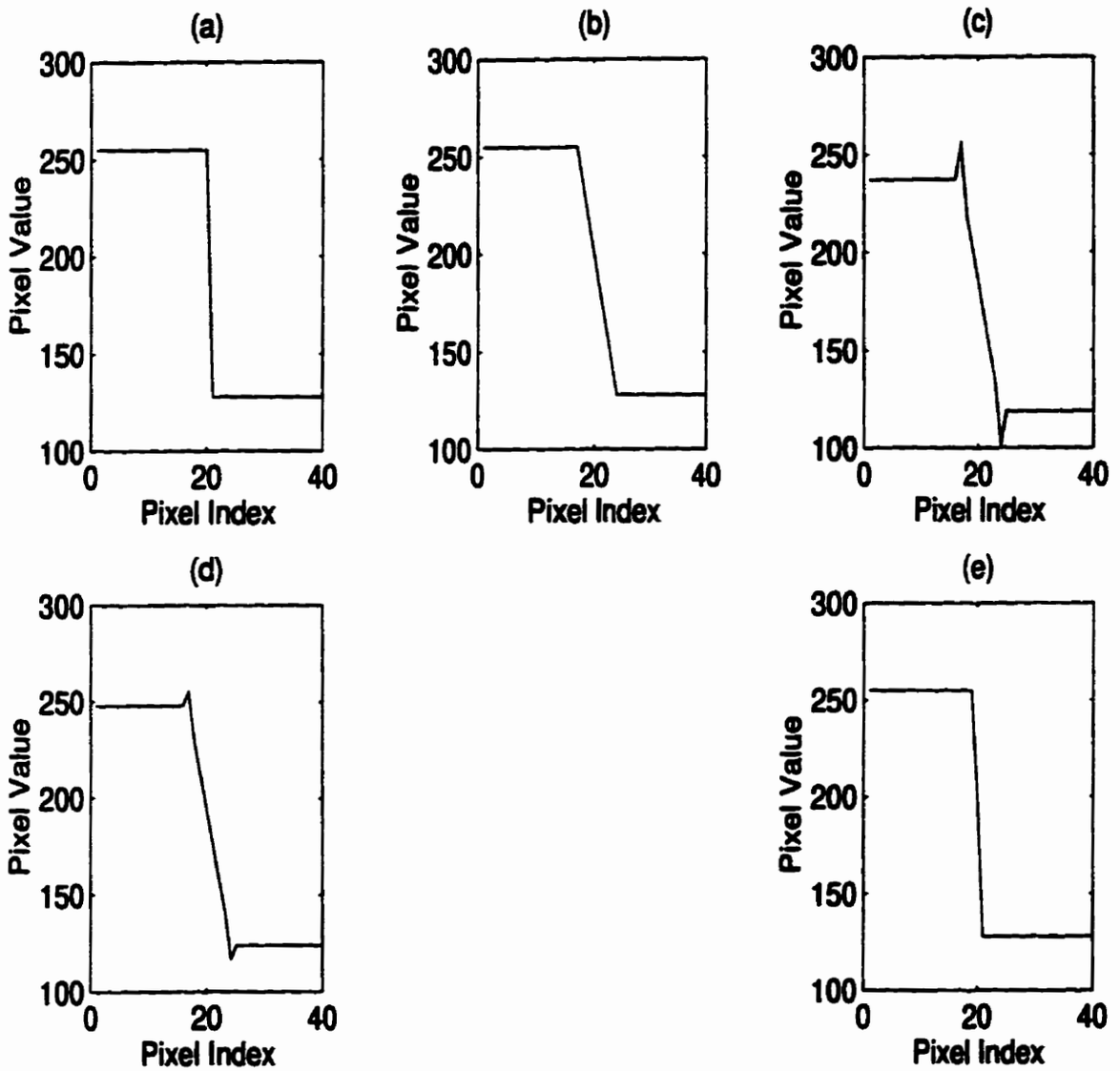

Figure 5.3. Edge profiles of the images in figure 5.1.

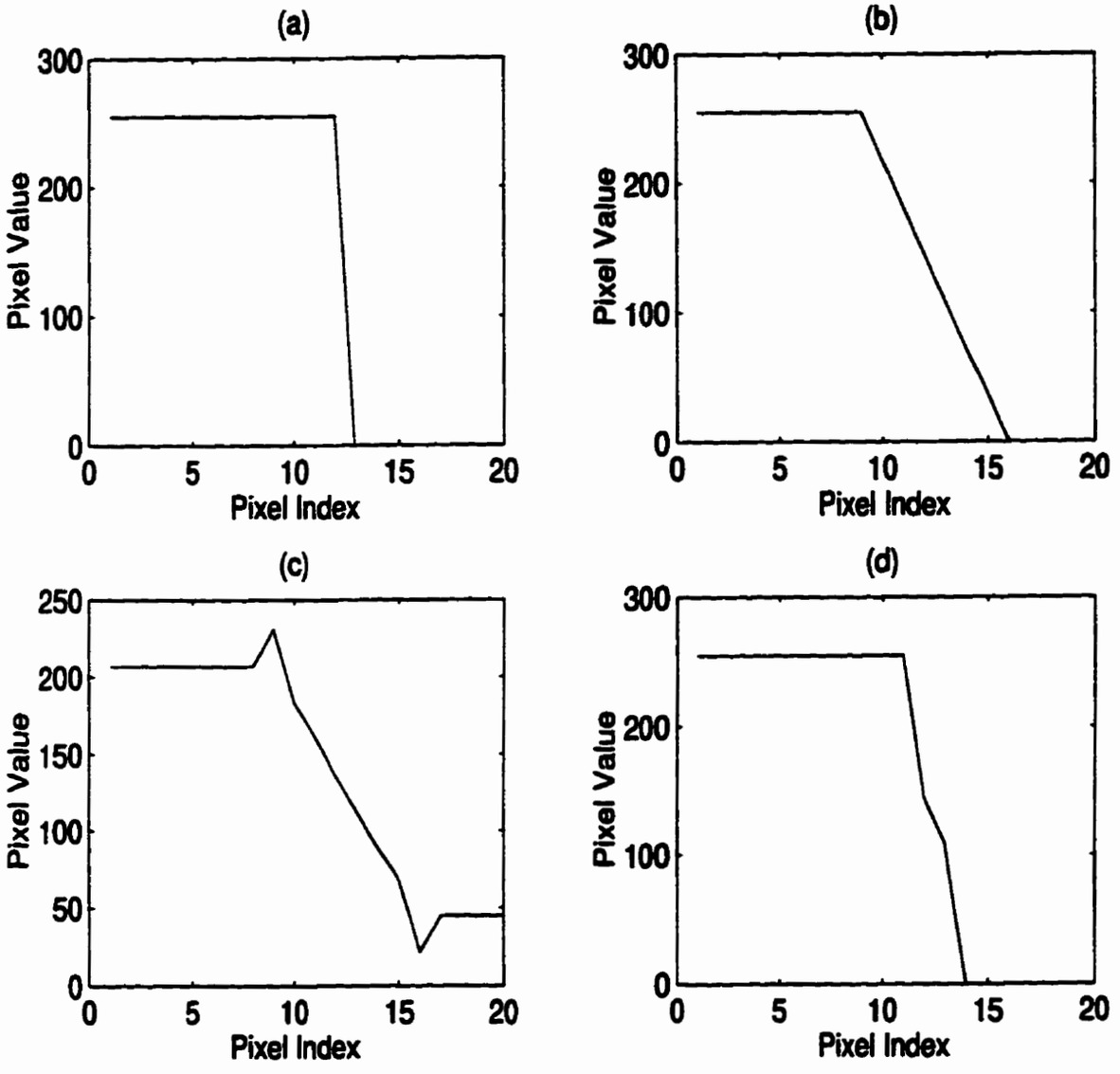

Figure 5.4. Edge profiles of the images in figure 5.2.

Image	Acutance times 100
Original	0.43
Blurred	0.16
Enhanced by subtracting Laplacian	0.23
Enhanced by unsharp masking	0.19
Enhanced by the proposed method	0.31

Table 5.1: Acutance values for the different versions of the synthesized square image in figure 5.1.

Region	Acutance times 100			
	Original image	Blurred image	Sharpened by subtracting Laplacian	Sharpened by the proposed method
1	0.59	0.34	0.40	0.46
2	0.56	0.22	0.23	0.36
3	0.71	0.32	0.45	0.50
4	0.75	0.28	0.34	0.46
5	0.70	0.04	0.37	0.47

Table 5.2: Acutance values for the different versions of the synthesized test image in figure 5.2.

CHAPTER 6

CONCLUDING REMARKS

6.1 Summary

This thesis evaluated adaptive-neighborhood or region-based image processing techniques. The techniques dealt with two different image processing problems: image restoration in the presence of multiplicative noise, and analysis and enhancement of edge-sharpness of objects present in an image.

6.1.1 Image Restoration

The discussion on image restoration started with a general review of selected existing noise filtering techniques. The filtering methods were categorized as local versus global methods and fixed versus adaptive methods. Four noise filtering methods were discussed in detail in chapter 2. The first three (the ATD LMS filter, the ARW LMS filter, and the ANNS filter) are adaptive filtering methods but designed to restore images with signal-independent additive Gaussian noise; these methods do not work well in the presence of signal-dependent multiplicative noise. The fourth method (the 3×3 multiplicative noise filter of Kuan et al.) is a fixed-neighborhood multiplicative filter which worked reasonably well in restoring images degraded by multiplicative noise.

In chapter 3, an AN filter for removing multiplicative noise was presented. Appli-

cation of the methods on the test images showed that fixed-neighborhood methods, as a result of lack of accommodation of nonstationary image statistics, often smooth the high-frequency information in the noisy image. The AN method, on the other hand, provides better approximation of local stationarity, better estimation of the signal and noise statistics, and hence improves noise reduction without blurring object edges. It was shown that repeated application of the AN method further improves the given image. It was also shown that the method works better as the ANs grown match more closely with the actual objects present in the image. The AN multiplicative noise filter was shown to produce better images than the other methods discussed (the mean and median filters, the ATD LMS filter, the ARW LMS filter, the ANNS filter, and the 3×3 multiplicative noise filter) in terms of both visual quality and MSE.

6.1.2 Edge Sharpness

In chapter 4, the focus was shifted to the measurement of edge sharpness. The need for a quantitative measure of edge sharpness was discussed first. Then, established methods of computing measures of edge sharpness or acutance were presented. The methods of Rangayyan and Elkadiki and El-faramawy et al. for computing acutance (IEPA) were discussed in detail. A modified formula for computing the IEPA was presented: the proposed method computes acutance on the basis of the continuous gradient along the normals to the ROI boundary pixels, instead of approximating the gradients by differences between corresponding pixels across the edge. The acutance

value computed by the method increases with increase in sharpness of the image and decreases with blurring.

Chapter 5 presented a region-based edge enhancement algorithm which aims at increasing IEPA, and hence at improving the edge sharpness of each object present in the image. At the beginning of the chapter, the importance of edge sharpness was reviewed again and the influence of the concept of edge sharpness on recent image processing techniques was discussed. A review of some fixed and adaptive edge sharpening methods for gray level images was presented. A method for improving edge sharpness in images of bi-level objects was proposed. In this method 1D operators are applied on the normal pixels at each boundary point of each object in the image. The operators are designed such that the differences between the foreground and the background pixels are increased, and hence the edges get sharper.

The proposed method sharpens the image by sharpening each object of the image separately instead of sharpening the image as a whole as is the case with most of the existing image sharpening algorithms. The method does not assume any a priori knowledge of the degraded image. The method was applied to increase the edge sharpness of bi-level images and it was shown that the method worked significantly better than conventional fixed-neighborhood sharpening methods; the observation was supported by increased acutance values of the enhanced regions.

6.2 Suggestions for Future Work

Although very good results have been obtained in this work in image restoration and edge enhancement, there are many areas which are open to further improvement. The ideas presented in this thesis may be extended and applied in many other existing image restoration and image enhancement problems.

The concept of the AN filter for restoring images with multiplicative noise can be extended to filter Poisson noise in nuclear medicine imaging and other types of signal-dependent noise. Further investigation is warranted towards developing more sophisticated region growing methods suited to different image and noise characteristics. Inclusion of a deblurring step to take into account shift-variant point spread functions would be the next logical, but more challenging, step.

For the continuous-gradient-based IEPA measurement, there are two limitations which can be examined in future research. The method is sensitive to noise as acutance increases slightly with the addition of noise. Also, the maximum value of acutance computed by the method, which occurs for a bi-level ROI, is less than 1.

For the method of region-based edge enhancement, more accurate algorithms for finding the normal pixels at sharp corners of ROIs and to the boundary of circular ROIs should be designed. The present method concentrates on improving edge sharpness only. In future work, the possibilities of enhancing or sharpening the interior details of regions with gray level variations by suitable modification of the present algorithm need to be explored. The effectiveness of the algorithm in enhancing natural and medical images should also be tested.

REFERENCES

[1] Walkup JF and Choens RC. Image processing in signal-dependent noise. *Optical Engineering*, 13:258–266, 1974.

[2] Arsenault HH, Gendron C, and Denis M. Transformation of film-grain noise into signal-independent additive Gaussian noise. *Journal of Optical Society of America*, 71:91–94, 1981.

[3] Froehlich GK, Walkup JF, and Asher RB. Optical estimation of signal-dependent noise. *Journal of Optical Society of America*, 68(12):1665–1675, 1978.

[4] Woods JW and Radewan CH. Kalman filtering in two dimensions. *IEEE Transactions on Information Theory*, IT-23(4):473–482, 1977.

[5] Chan P and Lim JS. One-dimensional processing for adaptive image restoration. *IEEE Transactions on Acoustics, Speech, and Signal Processing*, ASSP-33:117–126, 1985.

[6] Mahesh B, Song WJ, and Pearlman WA. Adaptive estimators for filtering noisy images. *Optical Engineering*, 29:489–494, 1990.

[7] Pratt WK. *Digital Image Processing*. Wiley-Interscience, New York, NY, 1978.

[8] Naderi F and Sawchuck AA. Estimation of images degraded by film-grain noise. *Applied Optics*, 17:1228–1237, April 1978.

[9] Lo CM and Sawchuck AA. Nonlinear restoration of filtered images with Poisson noise. In *Proceedings of SPIE Conference on Applied Digital Image Processing - III*, volume 207, pages 84–95, August 1979.

[10] Arsenault HH and Levesque M. Combined homomorphic and local-statistics processing for restoration of images degraded by signal-dependent noise. *Applied Optics*, 23(6):845–850, March 1984.

[11] Lee JS. Digital image enhancement and noise filtering by use of local statistics. *IEEE Transactions on Pattern Analysis and Machine Intelligence*, PAMI-2(2):165–168, March 1980.

[12] Lee JS. Refined noise filtering using local statistics. *Computer Graphics and Image Processing*, 15:380–389, 1981.

[13] Jiang SS and Sawchuck AA. Noise updating repeated Wiener filter and other adaptive noise smoothing filters using local image statistics. *Applied Optics*, 25(14):2326–2337, July 1986.

[14] Kalman RE. A new approach to linear filtering and prediction problems. *Transactions on ASME, Journal of Basic Engineering*, 82:35–45, 1960.

[15] Phillips DL. A technique for the numerical solution of certain integral equations of the first kind. *Journal of Association for Computing Machinery*, 9:84–97, 1962.

[16] MacAdam DP. Digital image restoration by constrained deconvolution. *Journal of Optical Society of America*, 60:1617–1627, December 1970.

[17] Hunt BR. The application of constrained least squares estimation to image restoration by digital computer. *IEEE Transactions on Computer*, C-22:805–812, September 1973.

[18] Oppenheim AV, Schafer RW, and Stockham Jr. TG. Nonlinear filtering of multiplied and convolved signals. *Proceedings of the IEEE*, 56:1264–1291, August 1968.

[19] Ingle VK, Radpour A, Woods JW, and Kaufman H. Recursive estimation with non-homogeneous image models. In *Proceedings of IEEE Pattern Recognition and Image Processing Conference*, pages 105–108, Chicago, IL, 1978.

[20] Ingle VK and Woods JW. Multiple model recursive estimation of images. In *Proceedings of IEEE International Conference on Acoustics, Speech, and Signal Processing*, pages 642–645, Washington, DC, 1976.

[21] Peyrovian MJ and Sawchuck AA. Restoration of noisy blurred images by a smoothing spline function. *Applied Optics*, 16:3147–3153, 1977.

[22] Rajala SA and de Figueiredo RJP. Adaptive nonlinear image restoration by a modified Kalman filtering approach. *IEEE Transactions on Acoustics, Speech, and Signal Processing*, ASSP-29:1033–1042, October 1981.

[23] Lev A, Zucker SW, and Rosenfeld A. Iterative enhancement of noisy images. *IEEE Transactions on Systems, Man, and Cybernetics*, SMC-7:435–442, 1977.

[24] Prager JM. Extracting and labeling boundary segments in natural scenes. *IEEE Transactions on Pattern Analysis and Machine Intelligence*, PAMI-2:16–27, 1980.

[25] Nagao M and Matsuyama T. Edge preserving smoothing. In *Proceedings of Fourth International Joint Conference on Pattern Recognition*, pages 518–520, Kyoto, Japan, 1978.

[26] Hadhoud MM and Thomas DW. The two-dimensional adaptive LMS (TDLMS) algorithm. *IEEE Transactions on Circuits and Systems*, 35:485–494, 1988.

[27] Mikhael WB and Ghosh SM. Two-dimensional variable step-size sequential adaptive gradient algorithms with applications. *IEEE Transactions on Circuits and Systems*, 38:1577–1580, 1991.

[28] Rabie TF. Adaptive-neighborhood and iterative methods for image restoration. Master's thesis, Dept. of Electrical and Computer Engineering, The University of Calgary, Calgary, Alberta, 1992.

[29] Song WJ and Pearlman WA. Restoration of noisy images with adaptive windowing and nonlinear filtering. In *Proceedings of SPIE Conference on Visual Communications and Image Processing*, volume 707, pages 198–206, 1986.

[30] Song WJ and Pearlman WA. A minimum-error minimum correlation filter for images. In *Proceedings of SPIE Conference on Applications of Digital Image Processing IX*, volume 697, pages 225–232, 1986.

[31] Paranjape RB, Rabie TF, and Rangayyan RM. Image restoration by adaptive neighborhood noise subtraction. *Applied Optics*, 33:2861–2869, 1994.

[32] Kuan DT, Sawchuck AA, Strand TC, and Chavel P. Adaptive noise smoothing filter for images with signal-dependent noise. *IEEE Transactions on Pattern Analysis and Machine Intelligence*, 7(2):165–177, March 1985.

[33] Gordon R and Rangayyan RM. Feature enhancement of film mammograms using fixed and adaptive neighborhoods. *Applied Optics*, 23(4):560–564, 1984.

[34] Gonzalez RC and Woods RE. *Digital Image Processing.* Addison-Wesley, Reading, MA, 1992.

[35] Morrow WM, Paranjape RB, Rangayyan RM, and Desautels JEL. Region-based contrast enhancement of mammograms. *IEEE Transactions on Medical Imaging*, 11(3):392–406, 1992.

[36] Paranjape RB, Rangayyan RM, Morrow WM, and Nguyen HN. Adaptive-neighborhood image processing. In *Proceedings of SPIE Conference on Visual Communications and Image Processing*, volume 1818, pages 198–207, 1992.

[37] Paranjape RB, Rangayyan RM, and Morrow WM. Adaptive neighborhood mean and median image filtering. *Journal of Electronic Imaging*, 3(4):360–367, 1994.

[38] Rangayyan RM and Elkadiki SG. Algorithm for the computation of region-based image edge profile acutance. *Journal of Electronic Imaging*, 4(1):62–70, 1995.

[39] Higgins GC and Jones LA. The nature and evaluation of the sharpness of photographic images. *Journal of Society of Motion Picture and Television Engineers*, 58:277–290, 1952.

[40] Wolfe RN and Eisen FC. Psychometric evaluation of the sharpness of photographic reproduction. *Journal of Optical Society of America*, 43(10):914–922, 1953.

[41] Perrin FH. Methods of appraising photographic systems part I: Historical review. *Journal of Society of Motion Picture and Television Engineers*, 69(3):151–156, 1960.

[42] Crane EM. An objective method for rating picture sharpness: SMT acutance. *Journal of Society of Motion Picture and Television Engineers*, 73:643–647, 1964.

[43] Gendron RG. An improved objective method for rating picture sharpness: CMT acutance. *Journal of Society of Motion Picture and Television Engineers*, 82:1009–1012, December 1973.

[44] Kriss MA. Image analysis of discrete and continuous systems: film and CCD sensors. In *Proceedings of SPIE Conference on CAN-AM Eastern '90*, volume 1398, pages 4–14, 1990.

[45] Higgins GC. Methods for analyzing the photographic system, including the effects of nonlinearity and spatial frequency response. *Journal of Photographic Science and Engineering*, 15(2):106–118, 1971.

[46] Higgins GC. Image quality criteria. *Journal of Applied Photographic Engineering*, 3(2):53–60, 1977.

[47] Hall EL. *Computer Image Processing and Recognition.* Academic Press, New York, NY, 1979.

[48] El-Faramawy NM, Rangayyan RM, Desautels JEL, and Alim OA. Adaptive computation of region-based image edge profile acutance. *Journal of Electronic Imaging (submitted)*, April 1996.

[49] Ventura JA and Chen JM. Segmentation of two-dimensional curve contours. *Pattern Recognition*, 25(10):1129–1140, 1992.

[50] Olabarriaga SD and Rangayyan RM. Subjective and objective evaluation of image sharpness-behavior of the region-based image edge profile acutance measure. In *Proceedings of SPIE Conference on Medical Imaging '96 (Image Perception)*, volume 2712, pages 154–162, 1996.

[51] Grossberg S. Neural dynamics of brightness perception: features, boundaries, diffusion, and resonance. *Perception and Psychophysics*, 36(5):428–456, 1989.

[52] Attenave F. Some information aspects of visual perception. *Psychological Review*, 61:183–193, 1954.

[53] Perona P and Malik J. Scale-space and edge detection using anisotropic diffusion. *IEEE Transactions on Pattern Analysis and Machine Intelligence*, 12(7):629–639, July 1990.

[54] Beghdadi A and Le Negrate A. Contrast enhancement technique based on local detection of edges. *Computer Vision, Graphics, and Image Processing*, 46:162–174, 1989.

[55] Cromartie R and Pizer SM. Edge affected context for adaptive contrast enhancement. In *Information Processing in Medical Imaging, 12th International Conference, IPMI Proceedings*, pages 474–485, July 1991.

[56] Marr D. *Vision.* WH Freeman, San Francisco, CA, 1982.

[57] Hildreth EC. The detection of the intensity changes by computer and biological vision systems. *Computer Vision, Graphics, and Image Processing*, 22:1–27, 1983.

[58] Van Vliet LJ, Young IT, and Beckers GL. A non-linear Laplace operator as edge detector in noisy images. *Computer Vision, Graphics, and Image Processing*, 45:167–195, 1989.

[59] Moron CJ. A morphological transformation for sharpening edges of features before segmentation. *Computer Vision, Graphics, and Image Processing*, 49:85–94, 1990.

[60] Saint-Marc P, Chen J, and Medioni G. Adaptive smoothing: A general tool for early vision. *IEEE Transactions on Pattern Analysis and Machine Intelligence*, 13(6):514–529, June 1991.